CRYPTOCHROME suppresses the circadian proteome and promotes protein homeostasis

Authors

David C.S. Wong[1], Estere Seinkmane[1], Alessandra Stangherlin[1], Aiwei Zeng[1], Nina M. Rzechorzek[1], Andrew D. Beale[1], Jason Day[2], Martin Reed[1], Sew Peak Chew[1], Marrit Putker[1,3] & John O'Neill[1].

Affiliations

[1]MRC Laboratory of Molecular Biology, Cambridge, UK.

[2]Department of Earth Sciences, University of Cambridge, Cambridge, UK.

[3]Current address: Hubrecht Institute, Utrecht, the Netherlands.

Correspondence to: oneillj@mrc-lmb.cam.ac.uk

Abstract

Circadian timekeeping in mammalian cells involves daily cycles of CRYPTOCHROME-dependent transcriptional feedback repression. Ablation of CRY in mice leads to reduced growth and numerous other phenotypes for reasons that are not well understood. Here, we find that cells adapt to CRY deficiency by extensive remodelling of the proteome, phosphoproteome and ionome, with twice the number of circadian-regulated proteins and phosphopeptides as well as increased rhythmic ion transport compared to wild-type cells. CRY-deficient cells also have increased protein synthesis and reduced proteasomal degradation, as well as an altered energetic state. These adaptations render cells more sensitive to stress, and may provide an explanation for the wide-ranging phenotypes of CRY-deficient mice. We suggest that daily rhythms in cellular protein abundance are damped by CRY-mediated repression to facilitate daily cycles of proteome renewal whilst maintaining protein homeostasis.

Introduction

From transcriptional activation and RNA processing, to protein synthesis, folding and degradation, multiple mechanisms operate at every stage of gene expression to ensure that each cellular protein is maintained in a concentration range appropriate for its biological function [1–3]. Proteome homeostasis is essential for cell viability and the correct temporal regulation of protein activity is critical to every biological process – too much or too little at the wrong time underlies most pathological states [4,5].

In mammals, cellular physiology is temporally orchestrated around daily cycles that regulate much of the proteome and most cellular functions to a circadian rhythm [6]. For example, global protein synthesis rates and ribosome biogenesis typically increase in anticipation of increased periods of animal activity (night-time in nocturnal mice, daytime in humans) [7,8]. Daily rhythms in proteome composition are observed *in vivo* and in cultured cells, under constant conditions, controlled by a cell-autonomous circadian clock [9,10]. In this way, circadian rhythms organise cell biology to anticipate and accommodate the predictable daily demands of day and night. Circadian dysregulation is strongly associated with pathological states [6], highlighting its importance for organismal health. Daily timekeeping is synchronised *in vivo* by systemic cues such as insulin and glucocorticoid signalling, which align internal cellular timing with environmental cycles [11]. On any given day, the circadian cycle is expressed by more cells of the human body than the cell division cycle, yet its mechanistic basis is poorly resolved [12].

Circadian rhythms in tissues and cultured cells are usually accompanied by daily oscillations in the abundance of many mRNAs [13]. These oscillations are mediated by daily cycles of transcriptional feedback repression of a core clock genetic circuit comprising the *Period1/2* and *Cryptochrome1/2* genes, and fine-tuned by various auxiliary but non-essential transcriptional feedback mechanisms [13,14]. Within this model, the transcription of *Period* and *Cryptochrome* genes is stimulated by a

complex containing the activating transcription factors (BMAL1 and CLOCK or NPAS2). The stability, interactions and nucleocytoplasmic shuttling of the encoded PER and CRY proteins is regulated post-translationally until, many hours later, they repress the activity of BMAL1-containing complexes. This transcriptional-translational feedback loop (TTFL) is proposed as the basis of circadian timekeeping in mammalian cells [15]. Genes whose transcription are regulated by core TTFL factors are thought to drive circadian rhythms in the encoded proteins to control myriad cellular functions [13,14].

Within the TTFL model of circadian rhythm generation, CRY proteins are the essential repressors of CLOCK/BMAL1 activity [16,17], and have long been considered indispensable for circadian rhythms *in vivo* and cells *ex vivo* [18–22]. In contrast, PER proteins play critical signalling and scaffolding roles, required for the nuclear import and targeting of CRY to BMAL1-containing complexes [17]. Recently however, we found that CRY-deficient cells, tissues and mice retain the capacity for circadian timing, in the absence of canonical TTFL function [23]. Similarly, circadian oscillations were retained in cells and tissue slices lacking BMAL1 [24]. Whilst we cannot exclude the presence of some unknown transcriptional feedback-driven oscillation, many previous observations argue against this [12,17,19,21,22,25–28]. Recent evidence supports the hypothesis that a conserved post-translational cytosolic oscillator (PTO, or “cytoscillator”) may be responsible for generating the oscillation from which circadian transcriptional cycles derive [12,29,30]. Thus, while the TTFL is crucial for rhythmic robustness and co-ordinating outputs, it is not required for generation of rhythms.

The complex phenotype of mice lacking CRY proteins has been interpreted to mean that circadian timekeeping is crucial for organismal physiology. The emerging observations that circadian rhythms are retained in CRY or BMAL1-deficient cells questions the basis of their respective knockout mouse phenotypes. We have therefore investigated the molecular consequences of CRY deficiency in cells

using an unbiased whole cell proteomic strategy. Our findings reveal a crucial role for CRY in the maintenance of protein homeostasis and suggest that the chronic stress-like state of CRY-deficient cells underlies the complex and numerous consequences of CRY deletion in mouse tissues and *in vivo*.

Results

Cell-autonomous rhythms in the proteome and phosphoproteome persist in the absence of CRY

To test the proteomic and phosphoproteomic consequences of CRY deletion, we used confluent primary mouse fibroblasts, a classic model of cellular circadian timekeeping where contact inhibition prevents any interference from the cell division cycle [9]. Wild-type (WT) and CRY1$^{-/-}$; CRY2$^{-/-}$ (CKO) mouse fibroblasts in cell culture were synchronised using daily temperature cycles and sampled under constant conditions (Figure 1A). Quantitative proteomics detected over 6000 proteins and around 4000 phosphopeptides in both cell types. As expected [19,21,31] CRY1 was selectively detected in WT cells and displayed a rhythmic abundance profile with delayed phase relative to a PER2 luciferase reporter (PER2::LUC) recorded from parallel replicate cultures (Figure S1A). Examples of rhythmic and arrhythmic proteins and phosphopeptides are shown in Figure S1B/C. Based on estimates of intrinsic noise of gene expression [32–36], we chose a threshold of 10% relative amplitude to define biological significance. However, there was no relative amplitude threshold chosen for rhythmic phosphopeptides due to the lack of similar studies.

In WT cells, 7% of detected proteins and 8% of detected phosphopeptides showed significant circadian abundance rhythms. Unexpectedly, 17% of detected proteins and 14% of phosphopeptides in CKO cells were rhythmically abundant (Figure 1B-E). There was a modest but significant difference in the median relative amplitude of protein rhythms in CKO cells compared with WT (Figure S1D). Amongst the minority of proteins that were rhythmically abundant in both genotypes (Figure 1C), there was a strong positive correlation between their relative amplitudes (Figure S1E), which were overall higher in CKO cells compared with WT (Figure 2A).

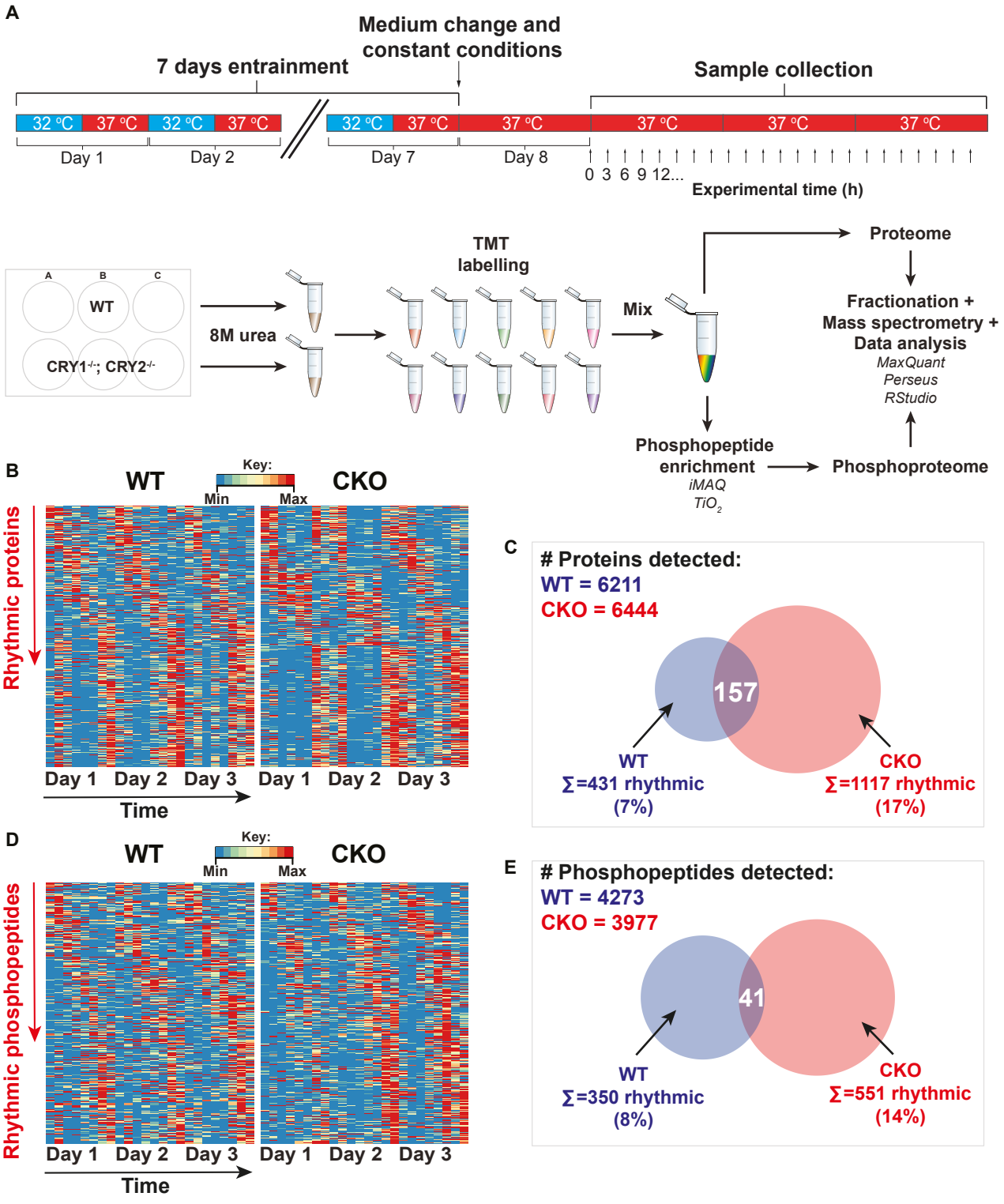

Figure 1: Cell-autonomous rhythms in the proteome and phosphoproteome persist in the absence of CRY. A) An overview of the proteomics experimental workflow. Samples were taken every 3 hours for 3 days in constant conditions, starting 24 h after medium change ("Experimental time 0 h"). **B)** Heatmaps showing min-max normalized plots for all the rhythmic proteins in WT (left) and CKO (right). For each genotype separately, rows represent proteins (sorted by phase), and each

column is a time point from the timecourse experiment. **C)** Venn diagram showing the numbers of rhythmic proteins in WT cells and CKO cells with relative amplitude ≥10%, with the overlap annotated. **D)** Heatmaps showing min-max normalized plots for all the rhythmic phosphopeptides in WT (left) and CKO (right). For each genotype separately, rows represent phosphopeptides (sorted by phase), and each column is a time point from the time-course experiment. **E)** Venn diagram showing the numbers of rhythmic phosphopeptides in WT cells and CKO cells, with the overlap annotated.

As with proteins, we found that CKO rhythmic phosphopeptides were significantly increased in relative amplitude and abundance compared with WT (Figure 2B). To gain more insight into the mechanism driving these phosphorylation rhythms we used the PHOSIDA database [37,38] to infer kinase activity using the rhythmic phosphopeptide sequences. Kinases typically associated with circadian period determination were not over-represented in WT or CKO rhythmic datasets compared to background however, nor in the set of phosphopeptides that were rhythmic in both genotypes (Figure S2 A-C).

The phase distribution of rhythmic proteins in both genotypes was clustered at experimental time 0 h (Figure 2C), when PER2::LUC activity in wild type cells was maximal (Figure S1A). This phase clustering was also true for proteins that were only rhythmic in CKO cells (Figure 2D), and for most proteins that were only rhythmic in WT cells (Figure 2E). A subset of proteins that were rhythmic in WT only, including CRY1, were clustered around experimental time 12 h (Figure 2E). This cluster was not present in proteins that were rhythmic in CKO only (Figure 2F). In WT cells, we observed clustering of protein phosphorylation to an earlier phase compared to rhythmically abundant proteins and PER2::LUC (Figure 2G). In comparison, there was a broader distribution of phase among rhythmic phosphopeptides in CKO cells (Figure 2H).

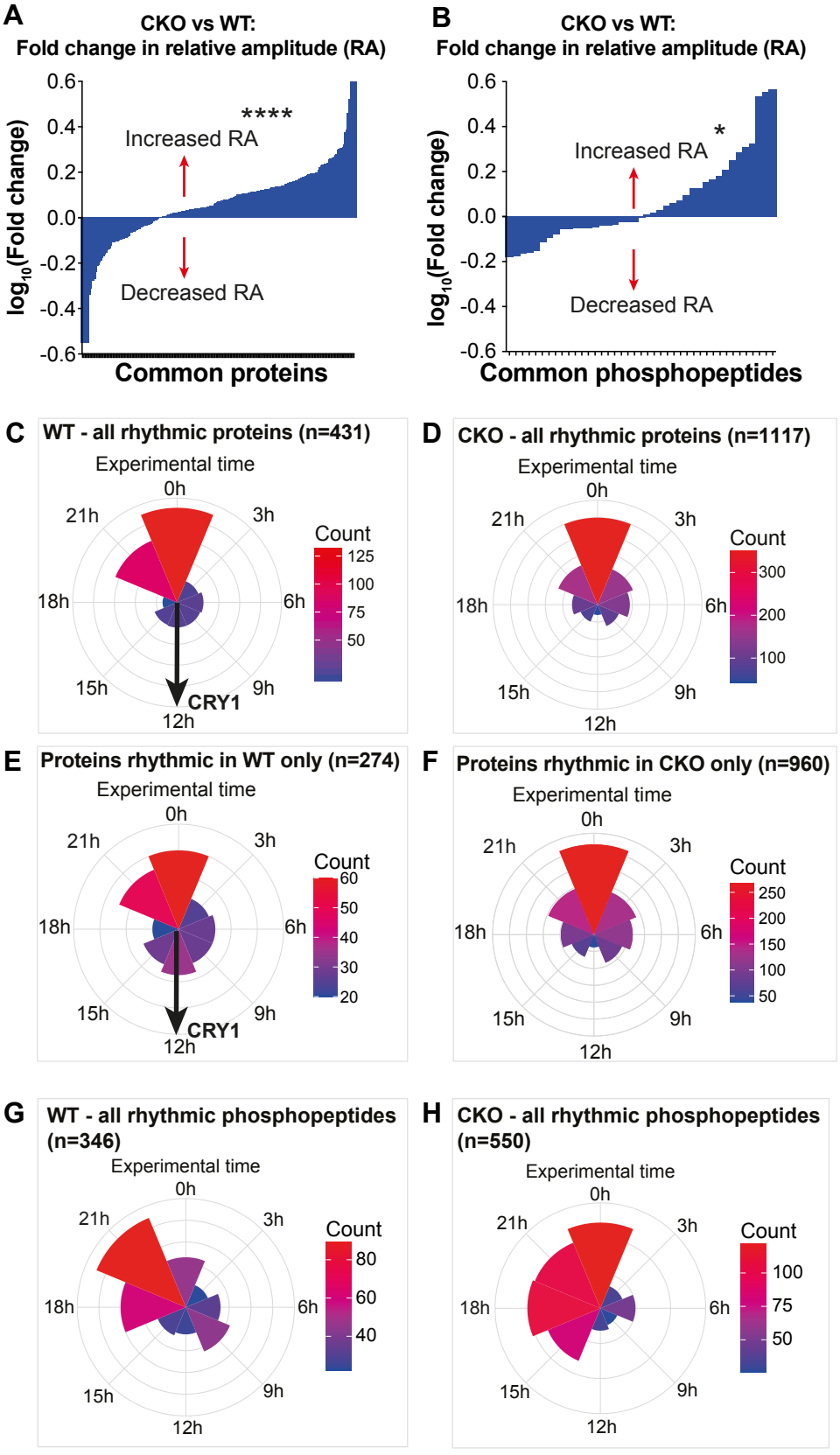

Figure 2: CRY regulates relative amplitude and phase of the rhythmic proteome and phosphoproteome. A) Fold-change in relative amplitude (RA) was calculated for each of the proteins found to be rhythmic in both genotypes by RAIN analysis (i.e. no RA cut-off). The mean fold change

(log) in RA was an increase of 14% in CKO cells compared to WT cells (One sample t-test, $p<0.0001$). **B)** Fold-change in relative amplitude (RA) was calculated for each of the phosphopeptides found to be rhythmic in both genotypes by RAIN. On average, the RA was increased in CKO cells compared to WT cells by 6% (One sample t-test, $p<0.05$). **C, D)** Circular histograms showing the number of proteins at each rhythmic phase. Phase is defined and estimated by RAIN, as the time of the first predicted peak in a 24-hour period. Concentric circles represent the counts scale, with the outermost circle marking the upper end of the counts. The distributions of rhythmic proteins in CKO cells was significantly different to WT cells (left, $p<0.001$, Watson's two-sample test). **E), F)** This was also the case for the proteins rhythmic in only one genotype (right, $p<0.001$, Watson's two-sample test). **G, H)** Circular histograms showing the number of phosphopeptides at each rhythmic phase. The distributions of rhythmic phosphopeptides in CKO cells was significantly different to WT cells ($p<0.001$, Watson's two-sample test).

These observations demonstrate that cell-autonomous rhythmicity of protein abundance and phosphorylation occurs independently of CRY, and hence the canonical TTFL. Instead, the primary role of CRY appears to be two-fold. First, CRY suppresses the amplitude of protein and phosphopeptide abundance rhythms. The greater amplitude in the absence of CRY reveals more than twice the number of rhythmic proteins detected in WT cells. Second, CRY regulates the phase of rhythmicity for a sub-population of proteins and phosphopeptides.

CRY suppresses the cell-autonomous rhythmic proteome and phosphoproteome

To gain insight into which aspects of cell physiology are most impacted by CRY deletion, we searched for patterns and commonalities among the set of dysregulated proteins. Although it has been suggested that proteins with shorter half-life have been correlated with circadian regulation [39], our analysis showed little or no obvious relationship in either WT or CKO cells. If anything, rhythmic proteins had longer half-lives than non-rhythmic proteins (Figure S3A, B). In contrast, rhythmic

166 proteins showed significantly higher average expression than non-rhythmic proteins (Figure 3A, B)
167 as previously suggested [40,41]. This relationship was true for both genotypes, but stronger in CKO
168 cells. Although part of this correlation may be due to preferential and more accurate detection of
169 oscillating high abundance proteins, this explanation cannot account for the different relationships in
170 WT and CKO cells (Figure 3C). We found similar relationships in the phosphoproteome (Figure 3D).
171 Thus, the TTFL-independent circadian rhythm seen in CKO acts preferentially towards more
172 abundant proteins and phosphopeptides.
173

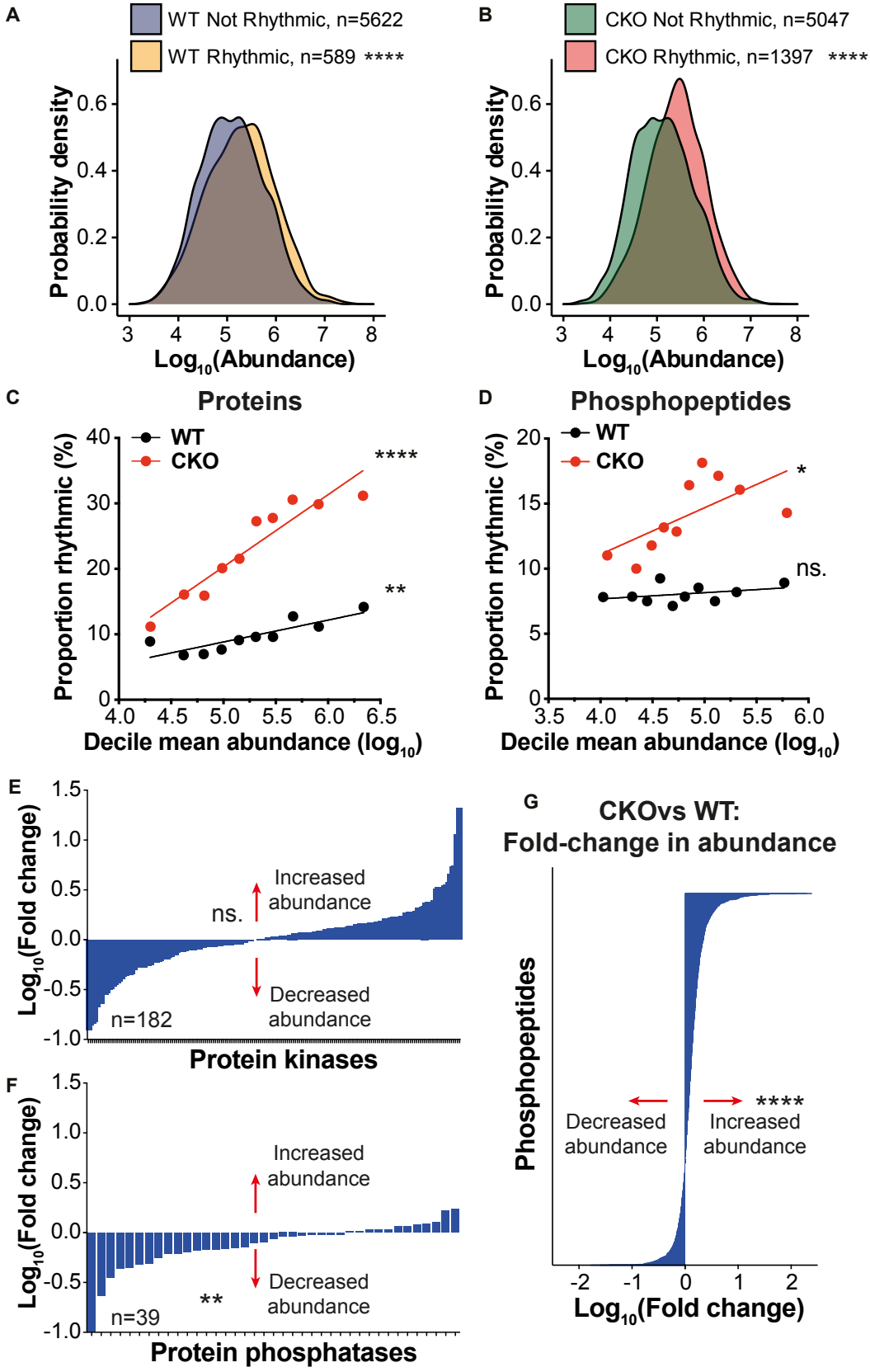

Figure 3. CRY suppresses the cell-autonomous rhythmic proteome and phosphoproteome. A), B) Probability density graphs compare the distribution of protein abundances. In both genotypes, rhythmic proteins were more abundant than non-rhythmic (WT $p<0.0001$, CKO $p<0.0001$, t-test with

log-transformed data). **C)** For each genotype, all proteins were divided into 10 deciles of equal number, ranked by abundance. The mean abundance of each decile was plotted against the proportion of the decile that was rhythmic. Linear regression lines are shown for each genotype, and the slopes were significantly non-zero (F test, WT $p=0.0016$, CKO $p<0.0001$). The slopes were also significantly different to each other (F test, $p=0.0001$). **D)** The same analysis in C) was carried out for phosphopeptides. The slopes was significantly non-zero in CKO but not WT (F test, WT $p=0.3$, CKO $p=0.04$). The slopes were also significantly different to each other (F test, $p<0.0001$). **E), F)** Fold-change in abundance was calculated for protein kinases (E) and protein phosphatases (F) detected in the proteomics dataset. There was a significant downregulation of phosphatase abundance in CKO cells compared to WT (One sample t test, $p=0.002$, $n=39$), but no overall change in kinase abundance (One sample t test, $p=0.7$, $n=182$). **G)** Fold-change in abundance was calculated for each phosphopeptide. There was a significant upregulation of phosphorylation in CKO cells compared to WT (One sample t test, $p<0.0001$, $n=2803$).

Overall, we observed that a remarkable 82% of the detected proteome in CKO cells were altered in abundance (Figure S3C, Abundance up + down), suggesting that global protein synthesis and degradation rates may be dysregulated. We therefore asked whether CRY deletion might unmask rhythmicity in proteins that normally exhibit similar rhythms of synthesis and degradation, thus appearing arrhythmic in WT cells. In our dataset there was a significant association between changes in abundance and changes in rhythmicity (Figure S3C). Our observations indicate that the cell-autonomous circadian clock regulates around 29% of the proteome (Figure S3C, green + blue + brown), with the TTFL primarily acting to suppress rhythms in the abundance of most of these proteins (Figure S3C, green). Similarly, we asked whether CRY deletion may impact upon the abundance of protein kinases and phosphatases, which act in dynamic equilibrium to determine the phosphorylation level of each phosphopeptide. In our proteomics dataset, there was no significant overall change in abundance of protein kinases (Figure 3E), but there was an overall decrease in

abundance of protein phosphatases (Figure 3F). Consistent with this, in our phosphoproteomics dataset we saw that overall there was an increase in phosphorylation (Figure 3G). We also found a strong link between changes in abundance and rhythmicity of phosphopeptides between the two genotypes (Figure S3D). This suggests that CRY represses global protein phosphorylation as well as rhythms in phosphorylation.

Bringing all these observations together, we suggest that CRY deletion may uncouple the synthesis and degradation of many proteins as well as the phosphorylation and dephosphorylation of many phosphosites. These two factors reveal more than twice the number of rhythmic proteins and phosphopeptides detected in WT cells, and results in a significant change in steady-state abundance of most of the proteome and phosphoproteome.

CRYPTOCHROME regulates proteasome activity and translation rate

We explored potential mechanisms for these widespread proteome changes by searching our dataset for key factors regulating protein synthesis and degradation. STAT3 and DDI2 are key regulators of proteasome abundance and activity [42]. We found their average expression levels were reduced in CKO cells (Figure 4A), accompanied by a striking reduction in the abundance of catalytic proteasomal subunits (Figure 4B, S4A) which we validated by western blot and enzymatic assays of proteasome activity (Figure 4C, S4B-C).

We also observed a significant increase in cytosolic protein synthesis rate by ^{35}S-methionine incorporation (Figure 4D, S4D-E). We considered that the combined effect of reduced proteasomal activity and increased translation rate would affect the overall steady state levels of cellular protein. We found this to be the case, with significantly higher overall protein per CKO cell compared with WT (Figure 4E).

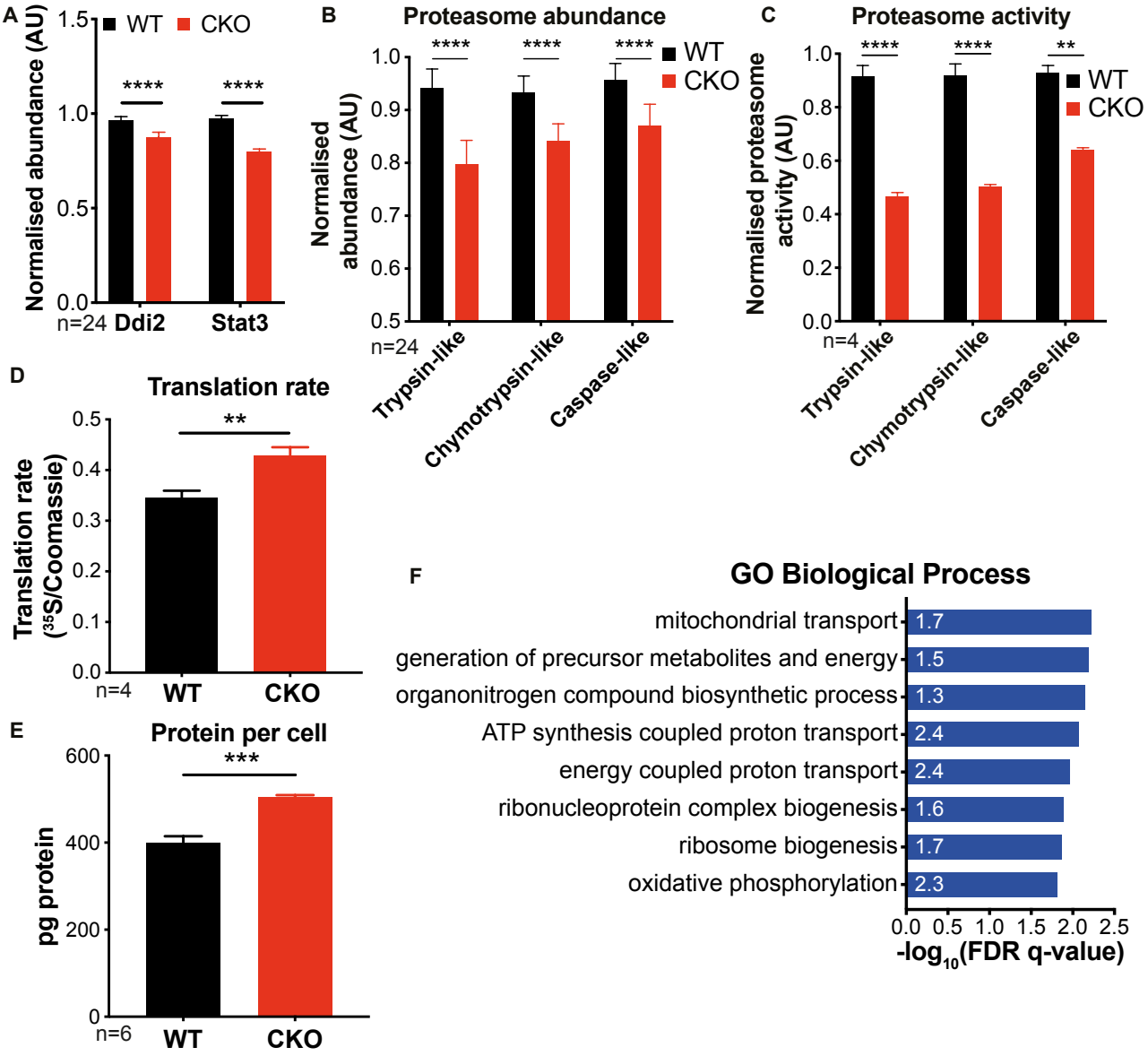

Figure 4. CRYPTOCHROME regulates proteasome activity and translation rate. A) The average abundance of proteins encoded by *Ddi2* and *Stat3* was calculated and max normalised for presentation. The average was calculated from all 24 time points of the proteomics experiment. Both proteins were down-regulated in CKO cells Mean±SD, multiple t tests with Holm-Sidak correction. **B)** The average abundance of catalytic proteasome subunits was calculated and max normalised for presentation. Trypsin-like (β2), chymotrypsin-like (β3) and caspase-like (β1) subunits are shown. The average was calculated from all 24 time points of the proteomics experiment. Mean±SD, 2-way ANOVA with Sidak's multiple comparisons. **C)** Proteasome activity measured using the ProteasomeGlo Assay (Promega). Mean±SEM, 2-way ANOVA with Sidak's multiple comparisons. N=6. **D)** Translation rate was measured using ^{35}S-methionine labelling and imaging with phosphor

screens (images shown in Figure S4). The quantification values were normalised to the total protein concentration as measured using Coomassie stain. Mean±SEM, Student's t test with Welch correction. N=3. **E)** Total protein mass per cell in confluent WT and CKO cultures. Cells were grown in two 12-well plates; one was used for cell counting and the other was used for lysis in RIPA buffer prior to protein quantification by BCA assay. Mean±SEM, Student's t test with Welch correction. **F)** The top results by FDR q-value, of ranked gene ontology analysis with all proteins ranked by decreasing fold change in abundance between CKO and WT cells. Fold-enrichment is annotated on each bar.

mRNA translation is one of the most energetically demanding of cellular processes, consuming up to 75% of the cellular ATP [1,43,44]. CKO cells showed increased abundance of proteins associated with ribosome biogenesis and energy generation which included many subunits of glycolytic and mitochondrial electron transport chain complexes as well as the F_0/F_1-ATP synthase (Figure 4F, S4F-H). Increased expression of proteins related to energy production may reflect an adaptation of CKO cells to accommodate the increased energetic demands of protein synthesis. Therefore cultured CKO cells have more protein, increased translation and decreased proteasomal degradation than WT cells, as well as an altered energetic state. Altogether, our data suggest that CKO cells likely maintain a different set point for protein homeostasis, as occurs in many pathological states [4,5].

Rhythmic regulation of ion transport and protein content is TTFL-independent and amplified by CRY deletion

We explored cellular processes that may be rhythmically regulated in CKO cells using gene ontology (GO) analysis. Of the rhythmically abundant proteins, ranked GO analysis revealed a consistent enrichment for processes associated with ion transport, both in wild type and CKO cells when analysed separately or combined (Figure 5A-C). In our proteomics dataset we also found altered expression levels and increased relative amplitudes of many ion transporters in CKO compared with

WT cells (Figure 5D-E). This included several members of the SLC12A family of electroneutral transporters (Figure 5F).

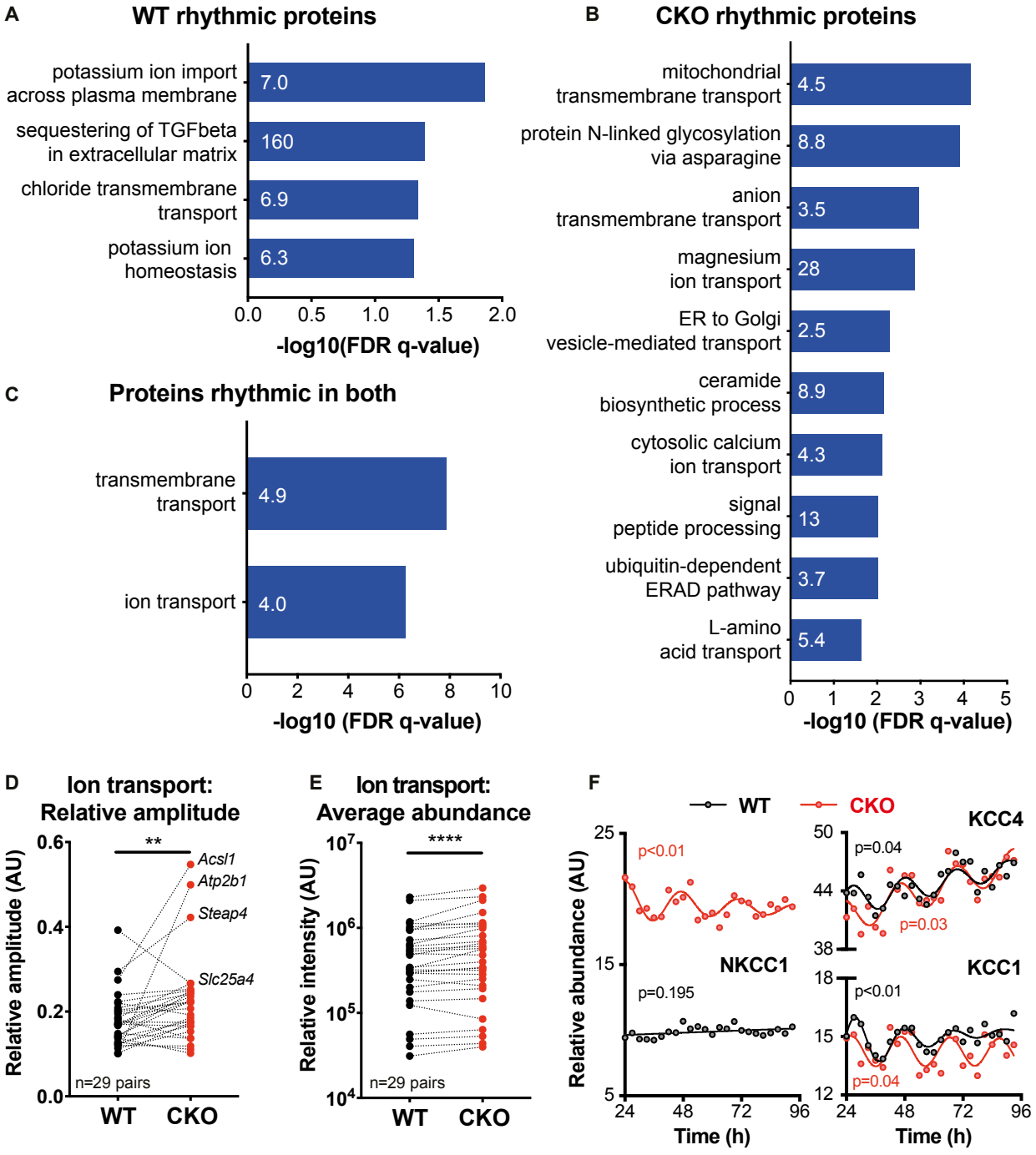

Figure 5. Rhythmic regulation of ion transport in WT and CKO cells. A) Gene ontology analysis for rhythmic proteins was carried out using Gene ontology enrichment analysis and visualisation (GOrilla) [45,46]. Significantly rhythmic WT proteins were compared against background (all proteins identified in the experiment), and the top non-overlapping GO Biological Process terms

shown, sorted according to FDR q-value. Fold enrichment is annotated on each bar. The same GO analysis was carried out comparing proteins rhythmic in both genotypes to the background **(B)** as well as all proteins that were rhythmic in CKO cells (C). **D), E)** 29 proteins were annotated as "Ion transport" by the GO analysis from the proteomics experiment – relative amplitude and average abundance was calculated for each of these proteins, in both WT and CKO. On average, both relative amplitude and average abundance was increased in CKO cells compared to WT (Paired t test). **F)** Examples of key ion transporters are shown, as detected in the proteomics experiment. P values show the results of an F test comparing fits of damped cosine against straight line. All proteins except WT NKCC1 had RAIN p-values <0.05.

To validate these findings, we measured the ion content of cells across the circadian cycle. Consistent with previous investigations (Stangherlin *et al*., submitted), in WT cells, K^+ and digitonin-extracted cytosolic protein concentrations exhibited anti-phasic circadian rhythms (Figure 6A), with no significant daily variation in total cellular protein. The same was observed in CKO cells (Figure 6B), but with higher relative amplitude (Figure 6C, D), and without observable rhythms in bioluminescence of the clock protein reporter, PER2::LUC (Figure 6A,B, bottom panel). In light of the enrichment we observed among CKO but not WT rhythmic proteins for Mg^{2+} and Ca^{2+} transport (Figure 5B), we also found it pertinent that these ions showed significant circadian variation in CKO, but not WT cells, whereas Mn^{2+} was rhythmic in neither (Figure S5). To understand the contribution of colloidal and ionic solutes to cytoplasmic osmolarity in our experiment we calculated the protein:ion ratio at each timepoint. We used K^+ levels as a proxy for ion content because it is the most abundant intracellular osmolyte. Protein:ion ratio was rhythmic, with CKO cells showing a higher average protein:ion ratio as well as a greater relative amplitude (Figure 6E-G). Considering our previous observations, the higher amplitude cytosolic protein rhythms in CKO cells likely drive the higher amplitude K^+ rhythms, because changing K^+ levels function through SLC12A transporter

299 activity to buffer cellular osmotic potential in response to changes in cytosolic macromolecular
300 content (Stangherlin *et al*., submitted).
301

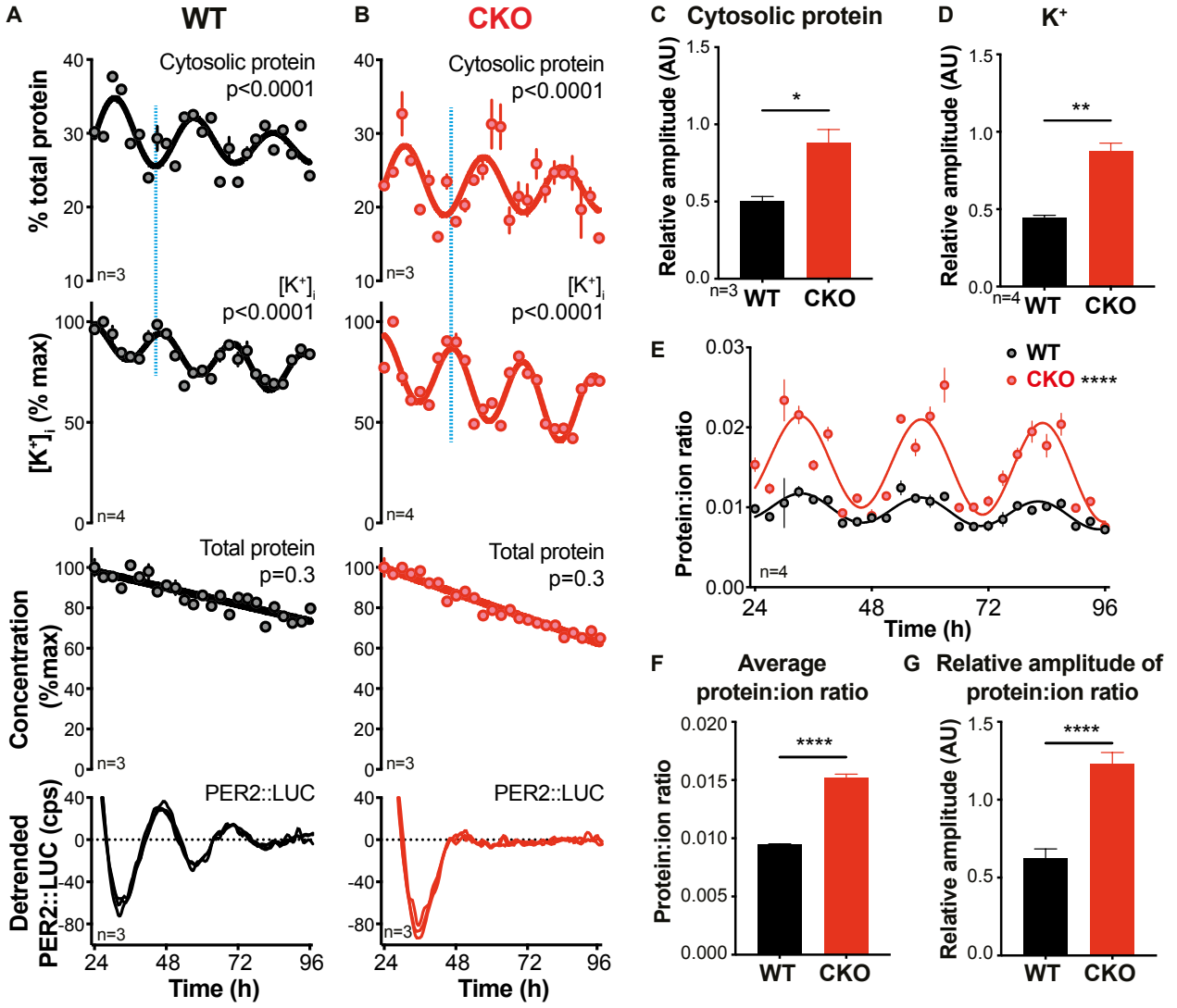

302

303 **Figure 6. CRY supresses rhythms of ion transport and osmotic balance. A), B)** From one time-
304 course experiment, ions, cytosolic proteins and total protein were extracted in parallel samples. The
305 presented experiment is representative of 3 separate time-course experiments that were carried out
306 (N=3). Blue lines indicate the anti-phasic oscillations in cytosolic protein and potassium
307 concentration. Mean±SEM, p-values from RAIN, red lines are fits by a damped cosine or a straight
308 line. Parallel PER2::LUC recordings were also performed and plotted as a phase marker. **C), D)**
309 Relative amplitudes of cytosolic protein and potassium concentrations oscillations in A) and B) were
310 greater in CKO compared to WT (Student's t test with Welch correction, mean±SEM). **E)** Protein:ion

ratio was calculated from the cytosolic protein and potassium concentrations in A) and B). For each time point, the average cytosolic protein concentration was divided by the potassium concentration of each biological replicate. Mean±SD. P-values were calculated by RAIN and annotated using asterisks in the legend. **F), G)** Average protein:ion ratio and relative amplitude was greater in CKO compared to WT (Student's t test with Welch correction, mean±SEM).

Our findings show that the rhythmic regulation of ion transport and cytosolic protein concentration may be of such fundamental importance to cell physiology that it is driven independently of CRY and therefore of canonical TTFL activity. Indeed, an important role of CRY may be to suppress daily changes in cytosolic macromolecular content and thus to efficiently maintain osmotic homeostasis. The loss of this function may be an important way in which protein homeostasis is altered in CKO cells compared to WT, since osmotic homeostasis is critical to cellular function and viability [47].

CRY-deficient cells are more sensitive to proteotoxic stress

The viability of CKO cells suggests that they can maintain protein homeostasis overall, despite the altered set point of protein homeostasis. Using ranked GO analysis of overall protein fold-changes compared with WT, we found that the expression of proteins involved in "response to stress" was increased in CKO cells (Figure 7A, S6A), suggesting that the proteostasis network in CKO cells is in an activated state [48–50].

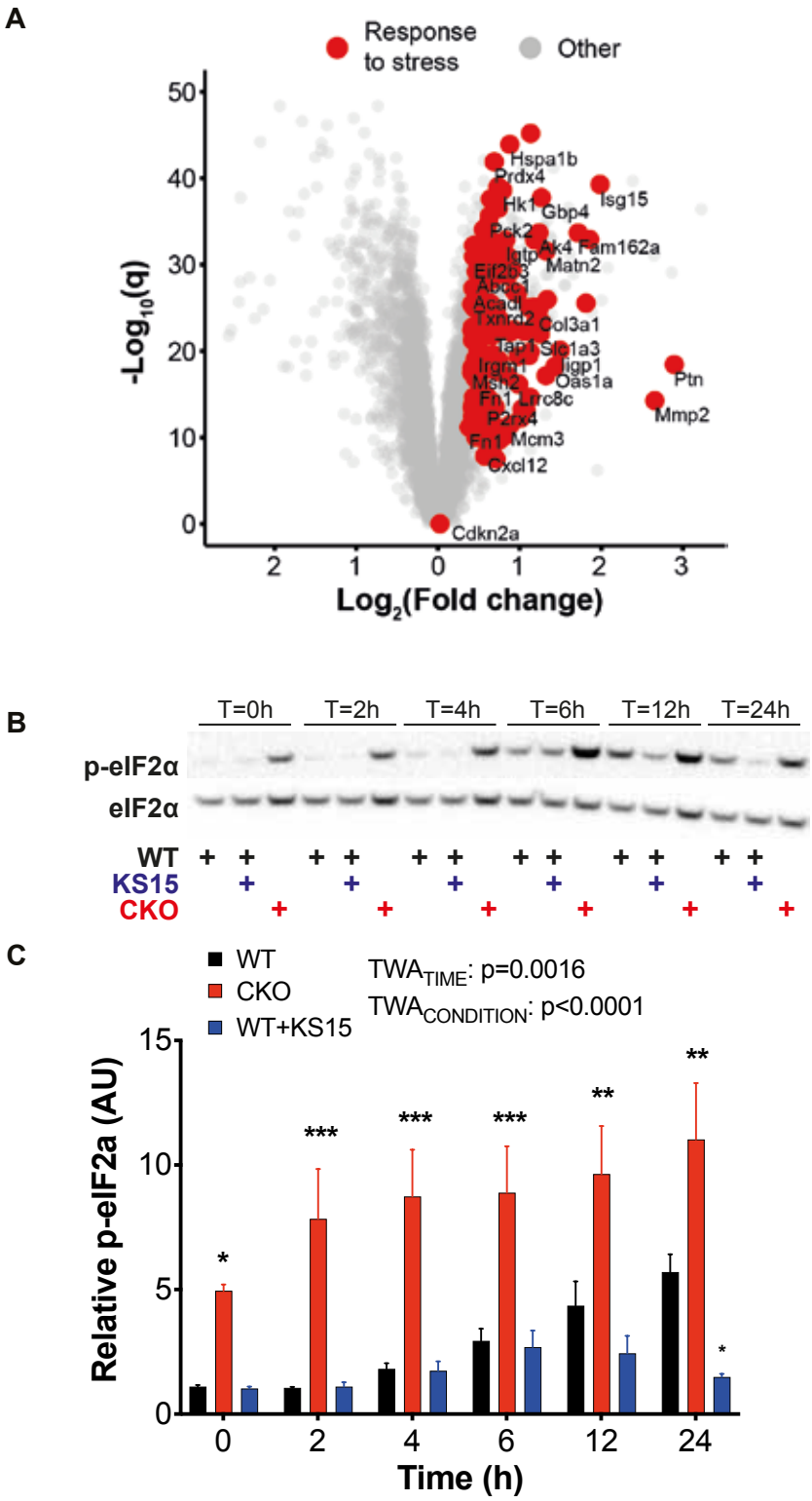

Figure 7. Increased stress in CKO cells. A) Volcano plot showing the fold change in average expression of all proteins in CKO cells compared to WT (q = Benjamini-Hochberg corrected p-value). Proteins annotated as "Response to stress" from GO analysis are highlighted in red, showing that these are upregulated in CKO cells. **B)** Cells treated with 500 nM tunicamycin (TUN) were lysed in RIPA buffer at time points from 2-24 hours. WT cells treated with 50 μM KS15 (CRY inhibitor)

were used as a control (see text). A representative western blot is shown, with probes against phosphorylated (above) and total (below) eIF2α. **C)** Quantification of the western blots in B), including all replicates. Mean±SEM, n=4. 2-way ANOVA p-values are reported. Asterisks indicate results of Holm-Sidak's multiple comparisons test vs. WT for each timepoint. WT cells also showed a linear trend by 1-way ANOVA ($p<0.0001$).

We therefore hypothesised that CKO cells may be more susceptible to perturbations that would elicit a proteotoxic stress response. To test this, we probed WT and CKO cells for phosphorylation of eIF2α, a well-characterised marker of the integrated stress response (ISR). As a control we treated cells with tunicamycin, which induces the ISR *via* inhibition of secretory pathway protein glycosylation [51,52]. We also treated cells with the CRY-inhibitor KS15 [53,54] to distinguish the acute effects of CRY inactivation from the long-term effects of its genetic deletion on cellular proteostasis. We found that CKO cells had higher basal levels of phosphorylated eIF2α compared with wild type or KS15 treated cells, as well as a significantly increased eIF2α phosphorylation following tunicamycin treatment (Figure 7B, C). Phosphorylation inactivates eIF2α in most cases to suppress translation [48], but we observed a net increase in protein synthesis in CKO cells (Figure 4D, S4D-E). Therefore the overall increase in translation rate must be higher than the suppression mediated by eIF2α phosphorylation.

From these observations we suggest that the altered set point of protein homeostasis in CKO renders them more susceptible to proteotoxic stress. Indeed, we found that even medium changes were sufficient to induce an increased stress response compared with WT cells (Figure S6B).

363 **Physiological consequences of CRY-deletion**

364 Given our observations we considered how the general change of protein homeostasis in CKO cells
365 might impact more broadly upon cellular and organismal physiology. Protein synthesis comprises the
366 most expensive portion of a cell's energy budget [1], and since we observed a net increased translation
367 rate in CKO cells we hypothesised that they may display increased energy consumption. Consistent
368 with this, we found that CKO cells had higher rates of glycolysis compared to WT cells (Figure 8A,
369 B).

370

371 Moreover, we also found features of increased energy usage in CKO mice. Both male and female
372 CKO mice displayed a reduced growth rate, despite increased food consumption (Figure 8C-E),
373 rescued by a single copy of *Cry2* in $Cry1^{-/-}; Cry2^{+/-}$ mice. This suggests that the increased energy
374 usage of cells that lack CRY may be a general cellular defect that affects the physiology of the animal.

375

376 Taking this further, we considered that the increased energy usage and susceptibility to proteotoxic
377 stress might lead to a general impairment of health in CKO mice. In a retrospective analysis of mouse
378 husbandry records we found a >3-fold increase in the death rate of weaned CKO mice compared with
379 isogenic WT controls, which was rescued in $Cry1^{-/-}; Cry2^{+/-}$ mice (Figure 8F). Post-mortem and
380 histopathology examinations were performed on 4 mice that underwent spontaneous death, and the
381 most common finding was mild extramedullary haematopoiesis (EMH), a sign of systemic
382 inflammation [55,56] (Table 1). This is consistent with previous observations of a pro-inflammatory
383 state in CKO mice [57–60]. Taking into account all our observations, we suggest that the increased
384 cellular energy usage coupled with impaired proteostasis may be a major contributor to the pleiotropic
385 physiological defects in CKO mice.

386

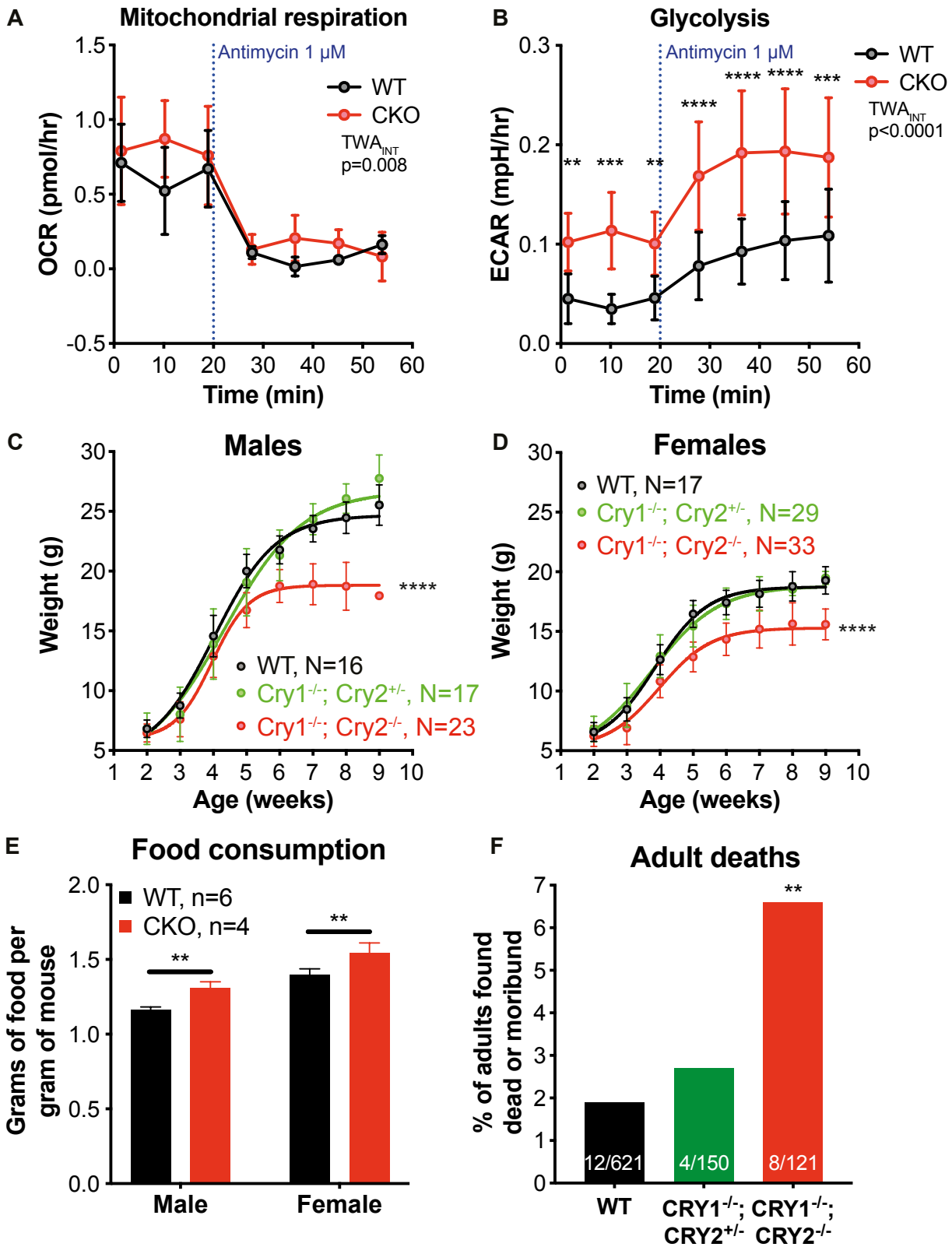

Figure 8. Metabolic and pathological consequences of CRY deletion. A), B) Seahorse assays were performed with WT and CKO cells in culture to measure oxygen consumption rate (OCR, A), which is a measure of mitochondrial respiration, as well as extracellular acidification rate (ECAR, B). The vertical blue line indicates that after 20 minutes of measurement, antimycin was added to halt

mitochondrial respiration. Mean±SEM, 2-way ANOVA with Holm-Sidak multiple comparisons test denoted by asterisks, N=3. **C), D)** Growth curves of male and female mice were weighed weekly. Mice were of the following genotypes: WT, $CRY1^{-/-}$; $CRY2^{+/-}$ and $CRY1^{-/-}$; $CRY2^{-/-}$ (CKO). F test was used to test the null hypothesis that one curve fits all sets. P values annotated as asterisks. **E)** Food consumption measured over 1 week, normalised for mouse weight. Food consumption was monitored by weighing food daily. Mean±SD, 2-way ANOVA. **F)** Death rates among the 3 genotypes mentioned above, expressed as a percentage of the number of mice. The absolute numbers of deaths and total population size are annotated on the bars. Only mice that had been weaned were included, and unnatural causes of death (e.g. cage flooding, fighting) were excluded. Asterisk indicates significance from Chi-squared test for trend, p=0.007. Comparing WT and CKO, Fisher's exact test p=0.009. Comparing WT and Het, Fisher's exact test p=0.5.

Mouse ID	Sex	Age at death (weeks)	Report findings
1	M	3	**EMH**, neutrophilic inflammation in lungs
2	F	0.3	**EMH**, low liver glycogen, bilateral hydronephrosis
3	F	8	**EMH**, bilateral hydronephrosis
4	F	20	**EMH**, severe lower urinary tract inflammation

Table 1: Histopathology of CRY-deficient mice. 4 histopathological examinations were carried out on mice that were moribund and culled as a result. All mice were confirmed $CRY1^{-/-}$; $CRY2^{-/-}$ by genotyping. Extra-medullary haematopoiesis (EMH) was found in all cases.

Discussion

We have shown that the absence of CRY does not abolish circadian organisation of the cellular proteome and phosphoproteome. Moreover, in CRY-deficient (CKO) cells we found a remarkable proteome dysregulation, leading to an altered set point of protein homeostasis that renders cells more susceptible to proteotoxic stress. This may be a general cellular feature that contributes to the pathophysiological state of CKO mice. These findings have significant implications for the role of the canonical TTFL and opens up several important avenues for future study.

There is accumulating evidence showing that the cell-intrinsic capacity to sustain ~24h rhythms does not require the canonical TTFL, and is generated post-translationally [12,24–28,61,62]. Instead the major contribution of CRY-mediated transcriptional-translational feedback to daily timing is to confer robustness upon the oscillation; indeed, CRY-deficiency simply appears to be epistatic to the daily organisation of behaviour and physiology *in vivo* under most conditions [23]. Our findings add to this growing body of literature, showing that circadian regulation at the proteome level persists in the absence of CRY-mediated feedback repression.

When analysing the effects of ablating clock genes, it is important to consider both altered rhythmicity of proteins and altered overall levels of proteins [63]. The abundance of any protein is a function of a dynamic equilibrium between synthesis and degradation. Global rates of protein synthesis are circadian regulated *in vitro* and *in vivo* [7,8,64–66], whereas total cellular protein levels are not (Figure 6; Stangherlin *et al.*, submitted) [23]. Therefore one or more pathways for protein degradation should normally be circadian regulated, for which some supporting evidence exists [67–69]. Since most rhythmically abundant mRNAs do not encode rhythmically abundant protein [10,24,70–74] this indicates that for most proteins, their relative rates of synthesis and degradation are either constant or have sufficiently similar rhythms that their concentrations do not change over 24h.

435 In our study, a key observation was that roughly twice as many proteins and phosphopeptides were
436 rhythmic in CKO cells compared with WT, but only a small minority of rhythmic species were
437 common to both genotypes. We also found that significant changes in the overall abundance of a
438 given protein or phosphopeptide was associated with a change in rhythmicity. The parsimonious
439 interpretation of our findings is that CRY normally functions to suppress rhythms in the abundance
440 of a substantial proportion (19%) of cellular proteins by coupling rhythms of synthesis and
441 degradation (Figure S3C). Removing CRY unmasks the rhythm for these proteins. In most cases
442 (16%) this leads to a change in the abundance of that protein, due to the new equilibrium that results
443 from a change in the average rate of protein synthesis relative to degradation. A smaller proportion
444 of cellular proteins (6%) upon which CRY normally confers rhythmic abundance lose that rhythm
445 when CRY is absent, with most (5%) reaching a new equilibrium concentration for the same reason.
446 The resultant change in abundance of >20% rhythmically regulated proteins in CKO cells may result
447 in an adaptation that leads to a change in the composition of most of the rest of the proteome (57%)
448 to maintain cellular homeostasis (Figure S3C). Such profound remodelling of the proteome is likely
449 to arise as an indirect consequence of CRY-deficiency as opposed to the direct regulation of most
450 cellular proteins by CRY.
451
452 For decades it has been argued that the adaptive advantage of cellular circadian clocks is to anticipate
453 the differential demands of day and night, by turning on genes to accommodate predicted demand.
454 Protein synthesis is the most energetically expensive process that most cells undertake however, and
455 multiple mechanisms exist to inactivate and sequester proteins that are not required [1,75]. Intuitively
456 then, it makes sense that cells would expend energy to ensure a constant abundance of most proteins
457 – to be mobilised as and when needed. However costly though, damaged proteins do need to be
458 degraded and replaced to avoid deleterious consequences such as aggregation. We therefore
459 hypothesise that a fundamental advantage offered by the canonical TTFL is the temporal

consolidation of proteome renewal, matching synthesis and degradation rates to keep protein concentrations constant and maintain protein homeostasis overall.

In addition to regulating circadian rhythms, CRYs have also been reported to play a role in magnetoreception [76,77], autoimmunity [57], cell cycle progression [78], and DNA damage signalling [79], as well as regulation of membrane potential [80], phototransduction [80], synaptic plasticity [81], GPCR signalling [82]. CRYs are therefore seemingly multifunctional. However, CRYs have also been found to have functions in fundamental cellular process that may underlie many of these reports. For example, CRYs regulate the transcription of many genes directly [21,31] and indirectly through interactions with various nuclear receptors [83]. CRY proteins are also promiscuous E3 ligase adaptors which target >100 cellular proteins for ubiquitination by the SCF^{FBXL3} complex to be degraded by the proteasome. These targets include $CRL4^{COP1}$ [84], c-MYC [85], TLK2 [86], FOXO1 [87] and E2F family members. Finally, CRYs may also mediate a more general repression of BMAL1-stimulated translation [23,64,88]. Adding to this, we found that proteasome activity was reduced in CKO cells whilst translation rate was increased, indicating a general function of CRY in protein homeostasis regulation.

It is likely that these factors all contribute to the changes in protein abundance for 82% of the proteome, that we observed in CKO cells (Figure S3C). Our observations of increased energy production and ion transport may reflect adaptations to the remodelled proteome in these cells. This adapted state in CKO cells renders them more sensitive to proteotoxic stress. We found that compared to WT, CKO cells have increased protein abundance and reduced K^+ levels overall, as well as higher amplitude rhythms of cytosolic protein and K^+. Changes in soluble protein concentration require stoichiometrically larger changes in ion concentration to maintain osmotic homeostasis [89]. We therefore suggest that CKO cells may have an impaired ability to buffer changes in intracellular osmolarity, which may contribute to the sensitivity to stress [47,90].

The increased energy consumption of CKO cells, associated with impaired regulation of protein homeostasis and increased sensitivity to proteotoxic stress may have systemic consequences for the animals. We suggest that this broad range of consequences of CRY deletion may contribute to the pronounced pathophysiology previously reported in CKO mice. For example, other studies have also reported impaired body growth in CKO mice, along with dysregulated growth hormone release [91,92]. Furthermore, CKO mice have an altered response to high fat diet, characterised by increased insulin secretion and lipid storage in adipocytes [93]. Female CKO mice have impaired fertility, and this is thought to be age-dependent [94]. Finally, CKO mice have increased susceptibility to cancer, in multiple models for carcinogenesis [95–98]. It is likely that a combination of the loss of specific functions of CRY, and a general protein homeostasis function of the TTFL are responsible for these CKO mutant phenotypes, since many are not shared with other behaviourally arrhythmic circadian mutant mice [63,99,100]. Of course, further work will be required to assess how successfully the interpretation we propose accounts for the circadian function of CRYPTOCHROME *in vivo,* and that of transcriptional-translational feedback loops more generally.

In this investigation, we have not addressed the nature of the post-translational mechanism postulated to generate circadian rhythms in mammalian cells, which is discussed elsewhere [12,23]. We note, however, that oscillations of protein synthesis stimulate facilitatory metabolism and compensatory ion transport to maintain osmotic and protein homeostasis during the metabolic cycle of yeast cells [101]. The many mechanistic features shared between mammalian circadian rhythms and yeast respiratory oscillations may indicate a common ancestral origin [30].

In our kinase inference analysis, we were surprised not to find evidence supportive of circadian phosphorylation by casein kinase 1 or any of the other kinases implicated in the post-translational circadian regulation. Indeed, the very poor overlap in rhythmically phosphorylated proteins between the two genotypes, and between rhythmic phosphorylation and rhythmic protein in either genotype,

suggests that the circadian functions of this post-translational modification are likely to be context-dependent. As with the proteome, however, we did notice a highly significant association between change in rhythmicity and change in phosphopeptide abundance. If a similar interpretation to that which we propose for the proteome were true, it would imply that as much as 20% of protein phosphorylation is subject to cell-autonomous circadian regulation (Figure S3D), but in most cases it is matched by a dephosphorylation rhythm of similar phase and amplitude. Given the consolidation of phosphorylation rhythms around a temporal window that anticipates the active phase (Figure 2G), we speculate that the circadian regulation of dynamic steady state phosphorylation might confer more sensitive and rapid transduction of a given extracellular stimulus when received around the rest-to-active transition compared with 12 hours later. Future work will be required to test this hypothesis experimentally.

In conclusion, we have shown that CRY-dependent feedback mechanisms are not required for cell-autonomous circadian rhythms of protein abundance or phosphorylation in mammalian cells. Moreover, when CRY is present, it functions to suppress more abundance rhythms than it facilitates. Loss of CRY also creates an overall imbalance of the proteome, with reduced proteasome activity, increased protein synthesis and protein levels. Cells adapt to this genetic insult through increased energy expenditure, and by altering osmotic balance and proteome composition to achieve a different set point for protein homeostasis, that renders them more sensitive to proteotoxic stress. This state may in turn have physiological consequences for the whole animal. We propose that the principal utility of CRY-mediated feedback repression is to couple global protein synthesis and degradation rates, ensuring the temporal consolidation of proteome renewal without commensurate change in protein abundance.

538 **Methods**

539 **Mammalian cell culture**

540 All animal work was licensed by the Home Office under the Animals (Scientific Procedures) Act
541 1986, with Local Ethical Review by the Medical Research Council and the University of Cambridge,
542 UK. Fibroblasts homozygous for PER2::LUCIFERASE [102] were extracted from adult mouse lung
543 tissue and then serial passage was used as described previously to induce spontaneous
544 immortalisation [30,103]. Fibroblasts were cultured in Dulbecco's Modified Eagle Medium (DMEM),
545 supplemented with 100 units/ml penicillin, 100 µg/ml streptomycin (Gibco) and 10% FetalClone III
546 serum (HyClone, Thermo Fisher). All cells were confirmed to be free of Mycoplasma. Unless stated
547 otherwise, confluent cell cultures up to a maximum of 30 passages were used during experiments to
548 abolish any effects of cell division, since these cells display contact inhibition.

549

550 **General statistics**

551 P values are annotated in figures with asterisks, where the number of asterisks indicates the
552 significance: Ns = not significant; * = $p \leq 0.05$; ** = $p \leq 0.01$, *** = $p \leq 0.001$; **** = $p \leq 0.0001$.
553 Technical replicates are denoted as "n" in the figures or figure legends (e.g. n=3), and biological
554 replicates are denoted as "N". Statistical tests were carried out using Prism Graphpad 8 (San Diego,
555 Ca) or R v3.6.3.

556

557 **Longitudinal bioluminescent reporter experiments**

558 Data from longitudinal bioluminescence recordings were analysed using Prism Graphpad 8 (San
559 Diego, Ca). A 24-hour moving average was used to detrend data, and so circa-24 hour rhythms can
560 more easily be observed and measured. Detrending in this way removes changes in baseline that occur
561 on a timescale greater than a day; 24-hour rhythms cannot be introduced by this method. Then a
562 circadian damped cosine wave was fitted by least-squares regression to determine period, phase and
563 amplitude. The formula is as follows:

564 $$y = (mx + c) + a\, e^{-kx} \cos\left(\frac{2\pi x - r}{p}\right)$$

565

566 Where *m* is the baseline gradient, *c* is the displacement in the *y* axis, *k* is the damping rate, *a* is the
567 amplitude, *r* is the phase and *p* is the period. The first 24 hours of each recording were omitted because
568 this represents the transient effects of medium change on clock gene expression. Rhythmicity of
569 bioluminescence recordings was assessed by comparing the fit of this equation to the null hypothesis
570 of a straight line using the Extra sum-of-squares F test in Prism Graphpad 8 (San Diego, CA). If
571 fitting to the damped cosine was preferred ($p \leq 0.05$) then the recording was deemed "rhythmic".

572

573 **Timecourse experiments: general structure**

574 Cells were plated at a near-confluent density (roughly 27,000 cells per cm^2) and cultured in DMEM
575 with 10% FetalClone III serum for one week in a temperature-controlled incubator that was
576 programmed to oscillate between 32°C and 37°C, with transitions every 12 hours. The cells received
577 a medium change at the transition between 37°C and 32°C after 4 days. After another 3 days the cells
578 received another medium change at the same transition time into medium containing either 10% or
579 1% serum, and the incubator was programmed to remain at 37°C constantly. At this time, a subset of
580 cells received medium containing 1 mM luciferin, and these were placed into an ALLIGATOR for
581 bioluminescent recording. After 24 hours, sampling began, with 3 hour intervals, and continuing for
582 3 days. The time point of the first sample is known as "Experimental time 0", and all time points are
583 reported relative to this. The nature of the sampling varied according to the specific experiment, and
584 details are presented in separate sections.

585

586 **Proteomics and phosphoproteomics**

587 ***Sample preparation***

588 A timecourse was carried out as described above. At each timepoint cells were washed twice in ice
589 cold PBS and then lysed at room temperature in 100 µL lysis buffer (8 M urea, 20 mM Tris, pH 8)

for 20 minutes. The lysis buffer was prepared the day before sampling began, and frozen in 1 mL aliquots. At each timepoint, one aliquot was defrosted at room temperature (23°C) whilst shaking at 700 rpm for 5 minutes. After lysis the cells were scraped and technical replicates were combined before flash freezing in liquid nitrogen and storage at -80°C.

After defrosting the samples were sonicated for 2 minutes and the protein concentration was measured using a BCA assay (Pierce). 12 pooled samples were created by combining a portion of each experimental sample such that each sample/pool contained an equal amount of protein. All samples were then flash frozen in liquid nitrogen and stored at -80ºC.

Enzymatic Digestion

Each sample (256 µg) was reduced with 5 mM DTT at 56°C for 30 minutes and then alkylated with 10 mM iodoacetamide in the dark at room temperature for 30 minutes. They were then digested with mass spectrometry grade Lys-C (Promega) at a protein:Lys-C ratio of 100:1 (w/w) for 4 hours at 25°C. Next, the samples were diluted to 1.5 M urea using 20 mM HEPES (pH 8.5) and digested at 30°C overnight with trypsin (Promega) at a ratio of 70:1 (w/w). Digestion was quenched by the addition of trifluoroacetic acid (TFA) to a final concentration of 1%. Any precipitates were removed by centrifugation at 13000g for 15 minutes. The supernatants were desalted using homemade C18 stage tips containing 3M Empore extraction disks (Sigma) and 5 mg of Poros R3 resin (Applied Biosystems). Bound peptides were eluted with 30-80% acetonitrile (MeCN) in 0.1% TFA and lyophilized.

TMT (Tandem mass tag) peptide labelling

The lyophilized peptides from each sample were resuspended in 100 µl of 2.5% MeCN, 250 mM triethylammonium bicarbonate. According to manufacturer's instructions, 0.8 mg of each TMT 10plex reagent (Thermo) was reconstituted in 41 µl of anhydrous MeCN. The peptides from each

616 time point and pooled sample were labelled with a distinct TMT tag for 75 minutes at room
617 temperature. The labelling reaction was quenched by incubation with 8 µl 5% hydroxylamine for 30
618 min. For each set of 10-plex TMT reagent, the labelled peptides from 8 time point samples + 2 pools
619 were combined into a single sample and partially dried to remove MeCN in a SpeedVac (Thermo
620 Scientific). After this, the sample was desalted as before and the eluted peptides were lyophilized.
621
622 ***Basic pH Reverse-Phase HPLC fractionation***
623 The TMT labelled peptides were subjected to off-line High Performance Liquid Chromatography
624 (HPLC) fractionation, using an XBridge BEH130 C18, 3.5 µm, 4.6 mm x 250 mm column with an
625 XBridge BEH C18 3.5 µm Van Guard cartridge (Waters), connected to an Ultimate 3000
626 Nano/Capillary LC System (Dionex). Peptide mixtures were resolubilized in solvent A (5% MeCN,
627 95% 10 mM ammonium bicarbonate, pH 8) and separated with a gradient of 1-90% solvent B (90%
628 MeCN, 10% 10 mM ammonium bicarbonate, pH 8) over 60 minutes at a flow rate of 500 µl/min. A
629 total of 60 fractions were collected. They were combined into 20 fractions and lyophilized and
630 desalted as before. 5% of the total eluate from each fraction was taken out for proteome LC-MS/MS
631 analysis and the rest was used for phosphopeptide enrichment.
632
633 ***Enrichment of phosphopeptides***
634 All 20 fractions of peptide mixture were enriched first using PHOS-Select iron affinity gel, an Iron
635 (III) Immobilised Metal Chelate Affinity Chromatography (IMAC) resin (Sigma). Desalted peptides
636 were resuspended in 30% MeCN, 0.25 M acetic acid (loading solution) and 30 µl of IMAC beads,
637 previously equilibrated with the loading solution, was added. After 60 minutes incubation at room
638 temperature, beads were transferred to a homemade C8 (3M Empore) stage tip and washed 3 times
639 with loading solution. Phosphopeptides were eluted sequentially with 0.4 M NH_3, 30% MeCN, 0.4
640 M NH_3 and 20 µl of 50% MeCN, 0.1% TFA.
641

642 The flow-through from the C8 stage tips was collected and combined into 10 fractions, and used for
643 titanium dioxide (TiO_2) phosphopeptide enrichment. For this, the total volume of flow-through was
644 made up to 50% MeCN, 2 M lactic acid (loading buffer) and incubated with 1-2 mg TiO_2 beads
645 (Titansphere, GL Sciences, Japan) at room temperature for 1 hour. The beads were transferred into
646 C8 stage tips, washed in the tip twice with the loading buffer and once with 50% MeCN, 0.1% TFA.
647 Phosphopeptides were then eluted sequentially with 50 mM K_2HPO_4 (pH 10) followed by 50%
648 MeCN, 50 mM K_2HPO_4 (pH 10) and 50% MeCN, 0.1% TFA.
649
650 The first 10 fractions of IMAC and the 10 fractions of TiO_2 enriched phosphopeptides were combined,
651 and the other 10 fractions from IMAC enrichment were combined into 5 fractions, thus making a
652 total of 15 fractions for phosphoproteomics analysis. Phosphopeptide solution from these fractions
653 were acidified, partially dried, and desalted with a C18 Stage tip that contained 1.5 µl of Poros R3
654 resin. These were then partially dried again and thus ready for mass spectrometry analysis.
655
656 ***LC MS/MS***
657 The fractionated peptides were analysed by LC-MS/MS using a fully automated Ultimate 3000 RSLC
658 nano System (Thermo) fitted with a 100 µm x 2 cm PepMap100 C18 nano trap column and a 75 µm
659 × 25 cm reverse phase C18 nano column (Aclaim PepMap, Thermo). Samples were separated using
660 a binary gradient consisting of buffer A (2% MeCN, 0.1% formic acid) and buffer B (80% MeCN,
661 0.1% formic acid), and eluted at 300 nL/min with an acetonitrile gradient. The outlet of the nano
662 column was directly interfaced via a nanospray ion source to a Q Exactive Plus mass spectrometer
663 (Thermo). The mass spectrometer was operated in standard data-dependent mode, performing a MS
664 full-scan in the m/z range of 350-1600, with a resolution of 70000. This was followed by MS2
665 acquisitions of the 15 most intense ions with a resolution of 35000 and Normalised Collision Energy
666 (NCE) of 33%. MS target values of 3e6 and MS2 target values of 1e5 were used. The isolation
667 window of precursor ion was set at 0.7 Da and sequenced peptides were excluded for 40 seconds.

668

669 ***Spectral processing and peptide and protein identification***

670 The acquired raw files from LC-MS/MS were processed using MaxQuant (Cox and Mann) with the
671 integrated Andromeda search engine (v1.6.3.3). MS/MS spectra were quantified with reporter ion
672 MS2 from TMT 10plex experiments and searched against the *Mus musculus* UniProt Fasta database
673 (Dec 2016). Carbamidomethylation of cysteines was set as fixed modification, while methionine
674 oxidation, N-terminal acetylation and phosphorylation (STY) (for phosphoproteomics group only)
675 were set as variable modifications. Protein quantification requirements were set at 1 unique and razor
676 peptide. In the identification tab, second peptides and match between runs were not selected. Other
677 parameters in MaxQuant were set to default values.

678

679 The MaxQuant output file was then processed with Perseus (v1.6.2.3). Reporter ion intensities were
680 uploaded to Perseus. The data was filtered: identifications from the reverse database were removed,
681 only identified by site, potential contaminants were removed and we only considered proteins with
682 ≥1 unique and razor peptide. Then all columns with an intensity "less or equal to zero" were converted
683 to "NAN" and exported as a .txt file.

684

685 The MaxQuant output file with phosphor (STY) sites table was also processed with Perseus software
686 (v1.6.2.3). The data was filtered: identifications from the reverse database were removed, only
687 identified by site, potential contaminants were removed and we only considered phosphopeptides
688 with localization probability ≥ 0.75. Then all columns with intensity "less or equal to zero" were
689 converted to "NAN" and exported as a .txt file.

690

691 ***Bioinformatics***

692 All data handling was done using R v3.6.3. Since the sample for timepoint 12 was missing for CRY1$^{-/-}$;
693 CRY2$^{-/-}$, abundance values were inferred for each protein by taking the mean of the two

694 neighbouring timepoints. WT and CKO datasets were analysed either combined or independently.
695 The combined analysis was used to directly compare protein and phosphopeptide abundances
696 between genotypes, since the internal reference scaling normalisation accounts for batch effects. The
697 independent method was used for all other analysis that did not require comparison of abundance,
698 thus allowing the detection of proteins that were present in one genotype but not the other.
699
700 Proteins and phosphopeptides were only accepted for further analysis if present in all timepoints and
701 pooled samples. Hence in the combined analysis, proteins/phosphopeptides had to be present in all
702 timepoints for both genotypes, as well as all pooled samples. In the independent analysis,
703 proteins/phosphopeptides had to be present in all timepoints and pools for one genotype only. Sample
704 loading normalisation was carried out by taking the sum of all intensities for each time point and
705 normalising to the mean of these, since an equal amount of protein was used for each TMT labelling
706 reaction. This was followed by internal reference scaling (IRS) to allow for comparisons between
707 TMT experiments [104]: for each TMT 10plex set the mean abundance for each protein in both pools
708 was calculated. Then the mean of these means was calculated and used to normalise the values for
709 each protein for all the samples.
710
711 Rhythmicity was tested using the RAIN (Rhythmicity Analysis Incorporating Non-parametric
712 methods) algorithm [105], and multiple testing was corrected for using the adaptive Benjamini-
713 Hochberg method. Proteins with a corrected $p \leq 0.05$ were deemed significant. Relative amplitude of
714 rhythmic proteins was calculated by detrending the data using a 24-hour moving average and dividing
715 the resultant range by the average normalised protein abundance. To include only proteins with a
716 biologically relevant level of oscillation, only those with relative amplitude $\geq 10\%$ were taken for
717 further analysis (see text for details). Phosphoproteomics data were handled in the same way, except
718 that normalised phosphopeptide abundances were adjusted according to the changes in abundance of

719 the corresponding protein from the normalised total proteome data, and no threshold for relative
720 amplitude was used.
721
722 Gene ontology analysis was performed using the GOrilla online tool [45,46]. Analysis was performed
723 either as a single ranked list of gene names, or as a target dataset compared to background (all proteins
724 detected in the experiment). Kinase recognition motifs were screened using a custom script written
725 in Python v2.7, which used the PHOSIDA database [37,38].
726
727 **Western blotting**
728 For Western blots, proteins were run on NuPAGE™ Novex™ 4-12% Bis-Tris Protein Gels (Thermo
729 Fisher) before transferring to nitrocellulose membranes. For transfer, the iBlot system (Thermo Fisher)
730 was used. Membranes were blocked using 5% milk powder (Marvel) or 0.125% BSA (Sigma) and
731 0.125% milk powder (Marvel) in TBS containing 0.1% Tween-20 (TBST) for 30 minutes at room
732 temperature then incubated with primary antibody at 4°C overnight. HRP-conjugated secondary
733 antibodies (Thermo Fisher) diluted 1:10000 in blocking buffer were incubated with the blots for 1
734 hour at room temperature. Chemiluminescence was detected in a Biorad chemidoc using Immobilon
735 reagent (Millipore). Protein loading was checked by staining gels with Colloidal Coomassie Blue
736 Stain (Severn Biotech). Densitometric analysis was carried out using Image Lab 4.1 (Biorad
737 Laboratories 2012).
738
739 **Measurement of cellular protein content**
740 At specified time points, confluent monolayers of cells were washed twice with ice-cold PBS. Cells
741 were then incubated with 200 µL digitonin lysis buffer (50 mM Tris pH 7.4, 0.01% digitonin, 5 mM
742 EDTA, 150 mM NaCl, 1 U/mL Benzonase, protease and phosphatase inhibitors) on ice for 15 minutes
743 before lysates were collected. For total protein extraction, cells were instead incubated with 200 µL
744 RIPA buffer (50 mM Tris pH 7.4, 1% SDS, 5 mM EDTA, 150 mM NaCl, 1 U/mL Benzonase,

745 protease and phosphatase inhibitors), on ice for 15 minutes. Cells lysed with RIPA buffer were then
746 scraped and collected and all samples were flash frozen in liquid nitrogen. After thawing, RIPA
747 lysates were sonicated at high power for 10 seconds at 4°C to shear genomic DNA. RIPA lysates and
748 digitonin lysates were clarified by centrifugation at 21,000 g for 15 minutes at 4°C.
749
750 Intrinsic tryptophan fluorescence was used to measure protein concentrations. 10 µL of each sample
751 was transferred into a UV-transparent 384 well plate (Corning 4681) in quadruplicate. After brief
752 centrifugation of the plate, quantification was carried out using a Tecan Spark 10M microplate reader,
753 with excitation at 280 nm and emission at 350 nm. Standards were made using bovine serum albumin
754 (Fisher Scientific), dissolved using the same lysis buffer as the lysates being measured. Standard
755 curves were fitted to a quadratic curve using Prism Graphpad 8 (San Diego, Ca), and protein
756 concentrations were interpolated.
757
758 **Measurement of intracellular ion content by Inductively Coupled Plasma - Mass Spectrometry**
759 **(ICP-MS)**
760 Confluent monolayers of cells were washed on ice with iso-osmotic buffer A (300 mM sucrose, 10
761 mM Tris base, 1 mM EDTA, pH 7.4 adjusted with phosphoric acid, 330-340 mOsm adjusted with
762 sucrose/HPLC water), followed by iso-osmotic buffer B (300 mM sucrose, 10 mM Tris base, 1 mM
763 EDTA, pH 7.4 adjusted with acetic acid, 330-340 mOsm adjusted with sucrose/HPLC water). Iso-
764 osmotic buffer A contains phosphoric acid which displaces lipid bound ions. Iso-osmotic buffer B
765 contains acetic acid which removes traces of phosphates. Cells were then incubated for 30 minutes at
766 room temperature in 200 µL ICP-MS cell lysis buffer (65% nitric acid, 0.1 mg/mL (100 ppb) cerium).
767 Lysates were then collected and stored at -80°C. All samples were thawed simultaneously and diluted
768 using HPLC water to a final concentration of 5% nitric acid. Diluted samples were analysed by
769 Inductively Coupled Plasma - Mass Spectrometry (ICP-MS) using the NexION 350D ICP-MS
770 (PerkinElmer Inc.) as described previously [8].

771

772 **Proteasome activity assays**

773 20,000 cells per well were plated in a 96-well plate using standard culture medium, and on the
774 following day the medium was changed. 10 μM epoxomicin in the medium was used as negative
775 control. 3 hours later, the ProteasomeGlo Cell-Based Assay (Promega) was used to measure
776 proteasome catalytic activity. Chymotrypsin-like, trypsin-like and caspase-like activities were
777 measured separately using the relevant substrates from Promega (Suc-LLVY-Glo, Z-LRR-Glo, Z-
778 nLPnLD-Glo respectively). Assay reagents were prepared according to the manufacturer's
779 instructions. The 96-well plate was equilibrated to room temperature, and a volume of assay reagent
780 equal to the volume of medium was added to each well before shaking at 700 rpm for 2 minutes. The
781 plate was incubated at room temperature for a further 10 minutes, and then luminescence was
782 measured using the Tecan Spark 10M microplate reader, recording counts for 1 second. The
783 luminescence readings from the epoxomicin controls represent background protease activity, and so
784 this was subtracted from all other recordings.

785

786 **Measurement of translation rate**

787 WT and CKO mouse lung fibroblasts were grown to confluence in 48-well plates, and medium was
788 changed 24h before the experiment to either low (1%) or high (10%) serum. The cells were pulsed
789 with 0.1 mCi/ml ^{35}S-L-methionine/^{35}S-L-cysteine mix (EasyTag™ EXPRESS35S Protein Labeling
790 Mix, Perkin Elmer) in cysteine/methionine-free DMEM for 15 min at 37°C, with or without serum
791 supplement. Afterwards, cells were washed with ice-cold PBS and lysed in digitonin-based buffer
792 (with protease inhibitor tablet, added freshly) on ice. Lysates were reduced with LDS buffer and run
793 on 4-12% Bis-Tris SDS-PAGE using MES buffer. Gels were then dried at 80°C and exposed
794 overnight to a phosphorimager screen. Images were acquired with Typhoon FLA700 gel scanner, and
795 quantified using Fiji.

796

For the puromycin pulse experiment, cells were seeded (in the presence of 1 mM luciferin) in fibronectin-coated dishes at high density one day before starting the experiment. Separate 6-well plates were used for each time point. 30 minutes before the start of the experiment, cells were synchronised by a dexamethasone pulse (10 nM), after which cells were exchanged into Air medium (DMEM without glucose, L-glutamine, phenol red, sodium pyruvate and sodium bicarbonate (Sigma). The following were added: 0.35 g/L sodium bicarbonate (Sigma), 5 g/L glucose (Sigma), 20 mM MOPS (VWR), penicillin/streptomycin solution (as above), Glutamax (Thermo Fisher), B27 (Thermo Fisher), 1 mM potassium luciferin solution (Biosyth), 1% FetalClone III serum. The medium was adjusted to pH 7.6 at room temperature, and osmolality adjusted to 350-360 mOsm/kg using sodium chloride). At the indicated time points, 10 µg/mL puromycin was added while keeping cells warm on a hot plate, after which the plate was incubated in tissue culture incubator for exactly 10 minutes. Timepoint 0 represents cells just before the dexamethasone pulse. Cells were then washed with ice-cold PBS, after which they were lysed in lysis buffer (50 mM tris, pH 7.5, 1% Triton X-100, 0.1% SDS, 1.5 mM $MgCl_2$, 100 mM NaCl, cOmplete protease inhibitor cocktail (Roche)) and flash frozen. For Western blot analysis, samples were spun down, diluted in Laemmli sample buffer, ran on 4-20% gradient gels, and blots were probed for ATF4 and tubulin.

Metabolic profiling of cells in culture

To characterise the metabolic profile of cells in culture metabolic assays from Seahorse Biosciences were used [106,107] to measure extracellular acidification rate (ECAR) and oxygen consumption rate (OCR) according to manufacturer's instructions (Agilent). 18,000 cells per well were plated in a 24-well cell culture microplate (Agilent) and incubated at 37°C overnight to adhere the cells. Empty wells in positions recommended by the manufacturer were used to assess background. Cells were then changed into warm "Seahorse medium" (DMEM without phenol red or bicarbonate, 4.5 g/L glucose, 1 mM pyruvate, 4 mM glutamine), and incubated for 30 minutes in a CO_2-free incubator at 37°C for equilibration. An Agilent Seahorse XFe24 Analyser was then used to measure OCR and

ECAR, with injection of antimycin diluted in Seahorse medium at a working concentration of 1 µM after the assay as a negative control.

Antibodies

Antibody name/target	Host species	Catalogue number	Manufacturer
Anti-mouse-HRP	Goat	A4416	Sigma
Anti-rabbit-HRP	Goat	A6154	Sigma
Anti-rat-HRP	Goat	629520	Thermo
Tubulin YL1-2	Rat		in-house
Proteasome 20S alpha 1-7	Mouse	ab22674	Abcam
EIF2a	Mouse	AhO0802	Thermo
P-EIF2a	Rabbit	ab32157	Abcam
ATF4 (CREB-2)	Mouse	sc-390063	Santa-Cruz Biotechnology
Histone H3	Rabbit	ab1791	Abcam

Acknowledgements

We thank biomedical technical staff at Medical Research Council (MRC) Ares facility and LMB facilities for assistance; G.T. van der Horst and J.S. Takahashi for sharing rodent models; Y-G. Suh, M.H. Hastings and E.S. Maywood for providing reagents and input; M. Hegde, E. Zavodszky, R. Edgar, N. Hoyle, M. Coetzee, J. Chesham, A. Hufnagel, P. Crosby, D.S. Tourigny, J.E. Chambers, H.C. Causton and Tim Stevens for assistance with analysis and experiments as well as valuable discussion. DCSW was supported by the MRC Doctoral Training Programme and the Frank Edward Elmore Fund. AS was supported by the AstraZeneca Blue Skies Initiative. NMR was supported by the Medical Research Council (MR/S022023/1). MP was supported by the Dutch Cancer Foundation (KWF, BUIT-2014-6637) and EMBO (ALTF-654-2014). JON was supported by the Medical Research Council (MC_UP_1201/4) and the Wellcome Trust (093734/Z/10/Z).

Contributions

DCSW, ES and JON designed the study, analysed the data and wrote the manuscript; DCSW, ES, AS, AZ and MP performed cell experiments; SPC and JD performed mass spectrometry analyses; DCSW, NMR, ADB and JON performed mouse studies; MR performed tissue collection and husbandry. All authors commented on the manuscript.

Conflicts of interest

The authors declare that they have no conflict of interest.

References

1. Wolff S, Weissman JS, Dillin A: **Differential Scales of Protein Quality Control**. *Cell* 2014, **157**:52–64.
2. Juszkiewicz S, Hegde RS: **Quality Control of Orphaned Proteins**. *Mol Cell* 2018, **71**:443–457.
3. Harper JW, Bennett EJ: **Proteome complexity and the forces that drive proteome imbalance**. *Nature* 2016, **537**:328–338.
4. Labbadia J, Morimoto RI: **The Biology of Proteostasis in Aging and Disease**. *Annu Rev Biochem* 2015, **84**:435–464.
5. Balchin D, Hayer-Hartl M, Hartl FU: **In vivo aspects of protein folding and quality control.** *Science* 2016, **353**:aac4354.
6. Cederroth CR, Albrecht U, Bass J, Brown SA, Dyhrfjeld-Johnsen J, Gachon F, Green CB, Hastings MH, Helfrich-Förster C, Hogenesch JB, et al.: **Medicine in the Fourth Dimension**. *Cell Metab* 2019, **30**:238–250.
7. Jouffe C, Cretenet G, Symul L, Martin E, Atger F, Naef F, Gachon F: **The Circadian Clock Coordinates Ribosome Biogenesis**. *PLoS Biol* 2013, **11**.
8. Feeney KA, Hansen LL, Putker M, Olivares-Yañez C, Day J, Eades LJ, Larrondo LF, Hoyle NP, O'Neill JS, van Ooijen G: **Daily magnesium fluxes regulate cellular timekeeping and energy balance**. *Nature* 2016, **532**:375–379.
9. Hoyle NP, Seinkmane E, Putker M, Feeney KA, Krogager TP, Chesham JE, Bray LK, Thomas JM, Dunn K, Blaikley J, et al.: **Circadian actin dynamics drive rhythmic fibroblast mobilization during wound healing**. *Sci Transl Med* 2017, **9**:eaal2774.
10. Reddy AB, Karp NA, Maywood ES, Sage EA, Deery M, O'Neill JS, Wong GKY, Chesham J, Odell M, Lilley KS, et al.: **Circadian Orchestration of the Hepatic Proteome**. *Curr Biol* 2006, **16**:1107–1115.
11. Crosby P, Hamnett R, Putker M, Hoyle NP, Reed M, Karam CJ, Maywood ES, Stangherlin A,

Chesham JE, Hayter EA, et al.: **Insulin/IGF-1 Drives PERIOD Synthesis to Entrain Circadian Rhythms with Feeding Time**. *Cell* 2019, **177**:896-909.e20.

12. Wong DC, O'Neill JS: **Non-transcriptional processes in circadian rhythm generation**. *Curr Opin Physiol* 2018, **5**:117–132.

13. Takahashi JS: **Transcriptional architecture of the mammalian circadian clock**. *Nat Rev Genet* 2016, **18**:164–179.

14. Ukai H, Ueda HR: **Systems Biology of Mammalian Circadian Clocks**. *Annu Rev Physiol* 2010, **72**:579–603.

15. Rosbash M: **The Implications of Multiple Circadian Clock Origins**. *PLoS Biol* 2009, **7**:e1000062.

16. Ye R, Selby CP, Chiou Y-Y, Ozkan-Dagliyan I, Gaddameedhi S, Sancar A: **Dual modes of CLOCK:BMAL1 inhibition mediated by Cryptochrome and Period proteins in the mammalian circadian clock.** *Genes Dev* 2014, **28**:1989–98.

17. Chiou Y-Y, Yang Y, Rashid N, Ye R, Selby CP, Sancar A: **Mammalian Period represses and de-represses transcription by displacing CLOCK-BMAL1 from promoters in a Cryptochrome-dependent manner.** *Proc Natl Acad Sci U S A* 2016, **113**:E6072–E6079.

18. Kume K, Zylka MJ, Sriram S, Shearman LP, Weaver DR, Jin X, Maywood ES, Hastings MH, Reppert SM: **mCRY1 and mCRY2 are essential components of the negative limb of the circadian clock feedback loop**. *Cell* 1999, **98**:193–205.

19. Sato TK, Yamada RG, Ukai H, Baggs JE, Miraglia LJ, Kobayashi TJ, Welsh DK, Kay SA, Ueda HR, Hogenesch JB: **Feedback repression is required for mammalian circadian clock function**. *Nat Genet* 2006, **38**:312–319.

20. van der Horst GT, Muijtjens M, Kobayashi K, Takano R, Kanno S, Takao M, de Wit J, Verkerk A, Eker a P, van Leenen D, et al.: **Mammalian Cry1 and Cry2 are essential for maintenance of circadian rhythms**. *Nature* 1999, **398**:627–30.

21. Ukai-Tadenuma M, Yamada RG, Xu H, Ripperger JA, Liu AC, Ueda HR: **Delay in feedback**

repression by cryptochrome 1 Is required for circadian clock function. *Cell* 2011, **144**:268–281.

22. Ode KL, Ukai H, Susaki EA, Narumi R, Matsumoto K, Hara J, Koide N, Abe T, Kanemaki MT, Kiyonari H, et al.: **Knockout-Rescue Embryonic Stem Cell-Derived Mouse Reveals Circadian-Period Control by Quality and Quantity of CRY1**. *Mol Cell* 2017, **65**:176–190.

23. Putker M, Wong D, Seinkmane E, Rzechorzek NM, Zeng A, Hoyle NP, Chesham JE, Edwards MD, Feeney KA, Fischer R, et al.: **CRYPTOCHROMES confer robustness, not rhythmicity, to circadian timekeeping**. *bioRxiv* 2020, doi:10.1101/2020.05.14.095968.

24. Ray S, Valekunja UK, Stangherlin A, Howell SA, Snijders AP, Damodaran G, Reddy AB: **Circadian rhythms in the absence of the clock gene Bmal1**. *Science (80-)* 2020, **367**:800–806.

25. Henslee EA, Crosby P, Kitcatt SJ, Parry JSW, Bernardini A, Abdallat RG, Braun G, Fatoyinbo HO, Harrison EJ, Edgar RS, et al.: **Rhythmic potassium transport regulates the circadian clock in human red blood cells**. *Nat Commun* 2017, **8**:1978.

26. Beale AD, Kruchek E, Kitcatt SJ, Henslee EA, Parry JSW, Braun G, Jabr R, von Schantz M, O'Neill JS, Labeed FH: **Casein Kinase 1 Underlies Temperature Compensation of Circadian Rhythms in Human Red Blood Cells**. *J Biol Rhythms* 2019, **34**:144–153.

27. O'Neill J, Reddy A: **Circadian clocks in human red blood cells**. *Nature* 2011, **469**:498–503.

28. Edgar RS, Green EW, Zhao Y, van Ooijen G, Olmedo M, Qin X, Xu Y, Pan M, Valekunja UK, Feeney KA, et al.: **Peroxiredoxins are conserved markers of circadian rhythms**. *Nature* 2012, **485**:459.

29. Hastings MH, Maywood ES, O'Neill JS: **Cellular Circadian Pacemaking and the Role of Cytosolic Rhythms**. *Curr Biol* 2008, **18**:R805–R815.

30. Causton HC, Feeney KA, Ziegler CA, O'Neill JS: **Metabolic Cycles in Yeast Share Features Conserved among Circadian Rhythms**. *Curr Biol* 2015, **25**:1056–1062.

31. Koike N, Yoo S-H, Huang H-C, Kumar V, Lee C, Kim T-K, Takahashi JS: **Transcriptional**

architecture and chromatin landscape of the core circadian clock in mammals. *Science* 2012, **338**:349–54.

32. Elowitz MB, Levine AJ, Siggia ED, Swain PS: **Stochastic gene expression in a single cell**. *Science (80-)* 2002, **297**:1183–1186.

33. Raser JM, O'Shea EK: **Control of stochasticity in eukaryotic gene expression**. *Science (80-)* 2004, **304**:1811–1814.

34. Volfson D, Marciniak J, Blake WJ, Ostroff N, Tsimring LS, Hasty J: **Origins of extrinsic variability in eukaryotic gene expression**. *Nature* 2006, **439**:861–864.

35. Sigal A, Milo R, Cohen A, Geva-Zatorsky N, Klein Y, Liron Y, Rosenfeld N, Danon T, Perzov N, Alon U: **Variability and memory of protein levels in human cells**. *Nature* 2006, **444**:643–646.

36. Pedraza JH, Van Oudenaarden A: **Noise propagations in gene networks**. *Science (80-)* 2005, **307**:1965–1969.

37. Gnad F, Gunawardena J, Mann M: **PHOSIDA 2011: The posttranslational modification database**. *Nucleic Acids Res* 2011, **39**:253–260.

38. Gnad F, Ren S, Cox J, Olsen J V., Macek B, Oroshi M, Mann M: **PHOSIDA (phosphorylation site database): Management, structural and evolutionary investigation, and prediction of phosphosites**. *Genome Biol* 2007, **8**.

39. Lück S, Thurley K, Thaben PF, Westermark PO: **Rhythmic Degradation Explains and Unifies Circadian Transcriptome and Proteome Data**. *Cell Rep* 2014, **9**:741–751.

40. Cheng Y, Chi Y, Zhang L, Wang GZ: **A single factor dominates the behavior of rhythmic genes in mouse organs**. *BMC Genomics* 2019, **20**:879.

41. Wang G-Z, Hickey SL, Shi L, Huang H-C, Nakashe P, Koike N, Tu BP, Takahashi JS, Konopka G: **Cycling Transcriptional Networks Optimize Energy Utilization on a Genome Scale.** *Cell Rep* 2015, **13**:1868–80.

42. Marshall RS, Vierstra RD: **Dynamic regulation of the 26S proteasome: From synthesis to**

degradation. *Front Mol Biosci* 2019, **6**:40.

43. Buttgereit F, Brandt MD: **A hierarchy of ATP-consuming processes in mammalian cells**. *Biochem J* 1995, **312**:163–167.

44. Rolfe DFS, Brown GC: **Cellular energy utilization and molecular origin of standard metabolic rate in mammals**. *Physiol Rev* 1997, **77**:731–758.

45. Eden E, Navon R, Steinfeld I, Lipson D, Yakhini Z: **GOrilla: A tool for discovery and visualization of enriched GO terms in ranked gene lists**. *BMC Bioinformatics* 2009, **10**.

46. Eden E, Lipson D, Yogev S, Yakhini Z: **Discovering motifs in ranked lists of DNA sequences**. *PLoS Comput Biol* 2007, **3**:0508–0522.

47. Danziger J, Zeidel ML: **Osmotic homeostasis**. *Clin J Am Soc Nephrol* 2015, **10**:852–62.

48. Pakos-Zebrucka K, Koryga I, Mnich K, Ljujic M, Samali A, Gorman AM: **The integrated stress response**. *EMBO Rep* 2016, **17**:1374–1395.

49. Kroemer G, Mariño G, Levine B: **Autophagy and the integrated stress response.** *Mol Cell* 2010, **40**:280–93.

50. Klaips CL, Jayaraj GG, Hartl FU: **Pathways of cellular proteostasis in aging and disease**. *J Cell Biol* 2018, **217**:51–63.

51. Heifetz A, Keenan RW, Elbein AD: **Mechanism of action of tunicamycin on the UDP-GlcNAc:dolichyl-phosphate GlcNAc-1-phosphate transferase**. *Biochemistry* 1979, **18**:2186–2192.

52. Oslowski CM, Urano F: **Measuring ER stress and the unfolded protein response using mammalian tissue culture system.** *Methods Enzymol* 2011, **490**:71–92.

53. Chun SK, Jang J, Chung S, Yun H, Kim NJ, Jung JW, Son GH, Suh YG, Kim K: **Identification and validation of cryptochrome inhibitors that modulate the molecular circadian clock**. *ACS Chem Biol* 2014, **9**:703–710.

54. Chun SK, Chung S, Kim HD, Lee JH, Jang J, Kim J, Kim D, Son GH, Oh YJ, Suh YG, et al.: **A synthetic cryptochrome inhibitor induces anti-proliferative effects and increases**

chemosensitivity in human breast cancer cells. *Biochem Biophys Res Commun* 2015, **467**:441–446.

55. Chiu SC, Liu HH, Chen CL, Chen PR, Liu MC, Lin SZ, Chang KT: **Extramedullary hematopoiesis (EMH) in laboratory animals: Offering an insight into stem cell research**. *Cell Transplant* 2015, **24**:349–366.

56. Johns JL, Christopher MM: **Extramedullary Hematopoiesis: A New Look at the Underlying Stem Cell Niche, Theories of Development, and Occurrence in Animals**. *Vet Pathol* 2012, **49**:508–523.

57. Cao Q, Zhao X, Bai J, Gery S, Sun H, Lin DC, Chen Q, Chen Z, Mack L, Yang H, et al.: **Circadian clock cryptochrome proteins regulate autoimmunity**. *Proc Natl Acad Sci U S A* 2017, **114**:12548–12553.

58. Hand LE, Hopwood TW, Dickson SH, Walker AL, Loudon ASI, Ray DW, Bechtold DA, Gibbs JE: **The circadian clock regulates inflammatory arthritis**. *FASEB J* 2016, **30**:3759–3770.

59. Lamia KA, Papp SJ, Yu RT, Barish GD, Uhlenhaut NH, Jonker JW, Downes M, Evans RM: **Cryptochromes mediate rhythmic repression of the glucocorticoid receptor**. *Nature* 2011, **480**:552–556.

60. Narasimamurthy R, Hatori M, Nayak SK, Liu F, Panda S, Verma IM: **Circadian clock protein cryptochrome regulates the expression of proinflammatory cytokines**. *Proc Natl Acad Sci U S A* 2012, **109**:12662–12667.

61. Millius A, Ode KL, Ueda HR: **A period without PER: understanding 24-hour rhythms without classic transcription and translation feedback loops.** *F1000Research* 2019, **8**.

62. Cho C-S, Yoon HJ, Kim JY, Woo HA, Rhee SG: **Circadian rhythm of hyperoxidized peroxiredoxin II is determined by hemoglobin autoxidation and the 20S proteasome in red blood cells**. *Proc Natl Acad Sci* 2014, **111**:12043–12048.

63. Yu EA, Weaver DR: **Disrupting the circadian clock: Gene-specific effects on aging, cancer,**

and other phenotypes. *Aging (Albany NY)* 2011, **3**:479–493.

64. Lipton JO, Yuan ED, Boyle LM, Ebrahimi-Fakhari D, Kwiatkowski E, Nathan A, Güttler T, Davis F, Asara JM, Sahin M: **The Circadian Protein BMAL1 Regulates Translation in Response to S6K1-Mediated Phosphorylation**. *Cell* 2015, **161**:1138–1151.

65. Jang C, Lahens NF, Hogenesch JB, Sehgal A: **Ribosome profiling reveals an important role for translational control in circadian gene expression**. *Genome Res* 2015, doi:10.1101/gr.191296.115.4.

66. Sinturel F, Gerber A, Mauvoisin D, Wang J, Gatfield D, Stubblefield JJ, Green CB, Gachon F, Schibler U: **Diurnal Oscillations in Liver Mass and Cell Size Accompany Ribosome Assembly Cycles**. *Cell* 2017, **169**:651-663.e14.

67. Desvergne A, Ugarte N, Radjei S, Gareil M, Petropoulos I, Friguet B: **Circadian modulation of proteasome activity and accumulation of oxidized protein in human embryonic kidney HEK 293 cells and primary dermal fibroblasts**. *Free Radic Biol Med* 2016, **94**:195–207.

68. Ma D, Lin JD: **Circadian regulation of autophagy rhythm through transcription factor C/EBPβ**. *Autophagy* 2012, **8**:124–125.

69. Ma D, Panda S, Lin JD: **Temporal orchestration of circadian autophagy rhythm by C/EBPβ**. *EMBO J* 2011, **30**:4642–4651.

70. Deery MJ, Maywood ES, Chesham JE, Sládek M, Karp NA, Green EW, Charles PD, Reddy AB, Kyriacou CP, Lilley KS, et al.: **Proteomic analysis reveals the role of synaptic vesicle cycling in sustaining the suprachiasmatic circadian clock.** *Curr Biol* 2009, **19**:2031–6.

71. Robles MS, Cox J, Mann M: **In-Vivo Quantitative Proteomics Reveals a Key Contribution of Post-Transcriptional Mechanisms to the Circadian Regulation of Liver Metabolism**. *PLoS Genet* 2014, **10**.

72. Mauvoisin D, Wang J, Jouffe C, Martin E, Atger F, Waridel P, Quadroni M, Gachon F, Naef F: **Circadian clock-dependent and -independent rhythmic proteomes implement distinct diurnal functions in mouse liver.** *Proc Natl Acad Sci U S A* 2014, **111**:167–72.

1032 73. Rey G, Milev NB, Valekunja UK, Ch R, Ray S, Santos MS Dos, Nagy AD, Antrobus R,
1033 MacRae JI, Reddy AB: **Metabolic oscillations on the circadian time scale in Drosophila**
1034 **cells lacking clock genes**. *Mol Syst Biol* 2018, **14**:e8376.
1035 74. Hurley JM, Jankowski MS, De Los Santos H, Crowell AM, Fordyce SB, Zucker JD, Kumar
1036 N, Purvine SO, Robinson EW, Shukla A, et al.: **Circadian Proteomic Analysis Uncovers**
1037 **Mechanisms of Post-Transcriptional Regulation in Metabolic Pathways.** *Cell Syst* 2018,
1038 **7**:613-626.e5.
1039 75. Hipp MS, Kasturi P, Hartl FU: **The proteostasis network and its decline in ageing**. *Nat Rev*
1040 *Mol Cell Biol* 2019, **20**:421–435.
1041 76. Bazalova O, Kvicalova M, Valkova T, Slaby P, Bartos P, Netusil R, Tomanova K, Braeunig
1042 P, Lee H-J, Sauman I, et al.: **Cryptochrome 2 mediates directional magnetoreception in**
1043 **cockroaches.** *Proc Natl Acad Sci U S A* 2016, **113**:1660–5.
1044 77. Gegear RJ, Foley LE, Casselman A, Reppert SM: **Animal cryptochromes mediate**
1045 **magnetoreception by an unconventional photochemical mechanism.** *Nature* 2010,
1046 **463**:804–7.
1047 78. Destici E, Oklejewicz M, Saito S, van der Horst GTJ: **Mammalian cryptochromes impinge**
1048 **on cell cycle progression in a circadian clock-independent manner.** *Cell Cycle* 2011,
1049 **10**:3788–97.
1050 79. Papp SJ, Huber AL, Jordan SD, Kriebs A, Nguyen M, Moresco JJ, Yates JR, Lamia KA: **DNA**
1051 **damage shifts circadian clock time via hausp-dependent cry1 stabilization**. *Elife* 2015,
1052 **2015**:1–19.
1053 80. Baik LS, Au DD, Nave C, Foden AJ, Enrriquez-Villalva WK, Holmes TC: **Distinct**
1054 **mechanisms of Drosophila CRYPTOCHROME-mediated light-evoked membrane**
1055 **depolarization and in vivo clock resetting.** *Proc Natl Acad Sci U S A* 2019, **116**:23339–
1056 23344.
1057 81. Damulewicz M, Mazzotta GM, Sartori E, Rosato E, Costa R, Pyza EM: **Cryptochrome Is a**

Regulator of Synaptic Plasticity in the Visual System of Drosophila melanogaster. *Front Mol Neurosci* 2017, **10**:165.

82. Zhang EE, Liu Y, Dentin R, Pongsawakul PY, Liu AC, Hirota T, Nusinow DA, Sun X, Landais S, Kodama Y, et al.: **Cryptochrome mediates circadian regulation of cAMP signaling and hepatic gluconeogenesis**. *Nat Med* 2010, **16**:1152–1156.

83. Kriebs A, Jordan SD, Soto E, Henriksson E, Sandate CR, Vaughan ME, Chan AB, Duglan D, Papp SJ, Huber A-L, et al.: **Circadian repressors CRY1 and CRY2 broadly interact with nuclear receptors and modulate transcriptional activity**. *Proc Natl Acad Sci* 2017, **114**:8776–8781.

84. Rizzini L, Levine DC, Perelis M, Bass J, Peek CB, Pagano M: **Cryptochromes-Mediated Inhibition of the CRL4Cop1-Complex Assembly Defines an Evolutionary Conserved Signaling Mechanism.** *Curr Biol* 2019, **29**:1954-1962.e4.

85. Huber AL, Papp SJ, Chan AB, Henriksson E, Jordan SD, Kriebs A, Nguyen M, Wallace M, Li Z, Metallo CM, et al.: **CRY2 and FBXL3 Cooperatively Degrade c-MYC**. *Mol Cell* 2016, **64**:774–789.

86. Correia SP, Chan AB, Vaughan M, Zolboot N, Perea V, Huber A-L, Kriebs A, Moresco JJ, Yates JR, Lamia KA: **The circadian E3 ligase complex SCFFBXL3+CRY targets TLK2**. *Sci Rep* 2019, **9**:198.

87. Jang H, Lee GY, Selby CP, Lee G, Jeon YG, Lee JH, Cheng KKY, Titchenell P, Birnbaum MJ, Xu A, et al.: **SREBP1c-CRY1 signalling represses hepatic glucose production by promoting FOXO1 degradation during refeeding**. *Nat Commun* 2016, **7**.

88. Lipton JO, Boyle LM, Yuan ED, Hochstrasser KJ, Chifamba FF, Nathan A, Tsai PT, Davis F, Sahin M: **Aberrant Proteostasis of BMAL1 Underlies Circadian Abnormalities in a Paradigmatic mTOR-opathy**. *Cell Rep* 2017, **20**:868–880.

89. Freedman J: *Cell Physiology Source Book*. Academic Press; 2012.

90. Hoffmann EK, Lambert IH, Pedersen SF: **Physiology of Cell Volume Regulation in**

Vertebrates. *Physiol Rev* 2009, **89**:193–277.

91. Bur IM, Cohen-Solal AM, Carmignac D, Abecassis PY, Chauvet N, Martin AO, van der Horst GTJ, Robinson ICAF, Maurel P, Mollard P, et al.: **The circadian clock components CRY1 and CRY2 are necessary to sustain sex dimorphism in mouse liver metabolism**. *J Biol Chem* 2009, **284**:9066–73.

92. Masuki S, Todo T, Nakano Y, Okamura H, Nose H: **Reduced α-adrenoceptor responsiveness and enhanced baroreflex sensitivity in Cry-deficient mice lacking a biological clock**. *J Physiol* 2005, **566**:213–224.

93. Barclay JL, Shostak A, Leliavski A, Tsang AH, Johren O, Muller-Fielitz H, Landgraf D, Naujokat N, van der Horst GTJ, Oster H: **High-fat diet-induced hyperinsulinemia and tissue-specific insulin resistance in Cry-deficient mice**. *AJP Endocrinol Metab* 2013, **304**:E1053–E1063.

94. Takasu NN, Nakamura TJ, Tokuda IT, Todo T, Block GD, Nakamura W: **Recovery from Age-Related Infertility under Environmental Light-Dark Cycles Adjusted to the Intrinsic Circadian Period**. *Cell Rep* 2015, **12**:1407–1413.

95. Chan AB, Lamia KA: **Cancer, hear my battle CRY**. *J Pineal Res* 2020, doi:10.1111/jpi.12658.

96. Kettner NM, Voicu H, Finegold MJ, Coarfa C, Sreekumar A, Putluri N, Katchy CA, Lee C, Moore DD, Fu L: **Circadian Homeostasis of Liver Metabolism Suppresses Hepatocarcinogenesis**. *Cancer Cell* 2016, **30**:909–924.

97. Lee S, Donehower LA, Herron AJ, Moore DD, Fu L: **Disrupting Circadian Homeostasis of Sympathetic Signaling Promotes Tumor Development in Mice**. *PLoS One* 2010, **5**:e10995.

98. Mteyrek A, Filipski E, Guettier C, Oklejewicz M, van der Horst GTJ, Okyar A, Lévi F: **Critical cholangiocarcinogenesis control by cryptochrome clock genes**. *Int J Cancer* 2017, **140**:2473–2483.

99. Maury E, Hong HK, Bass J: **Circadian disruption in the pathogenesis of metabolic**

syndrome. *Diabetes Metab* 2014, **40**:338–46.

100. Paschos GK, FitzGerald GA: **Circadian clocks and vascular function**. *Circ Res* 2010, **106**:833–841.

101. O'Neill J, Hoyle NP, Robertson JB, Edgar RS, Beale AD, Peak-Chew SY, Day J, Costa ASH, Frezza C, Causton HC: **Eukaryotic cell biology is temporally coordinated to support the energetic demands of protein homeostasis**. *bioRxiv* 2020, doi:10.1101/2020.05.14.095521.

102. Yoo S-H, Yamazaki S, Lowrey PL, Shimomura K, Ko CH, Buhr ED, Siepka SM, Hong H-K, Oh WJ, Yoo OJ, et al.: **PERIOD2::LUCIFERASE real-time reporting of circadian dynamics reveals persistent circadian oscillations in mouse peripheral tissues.** *Proc Natl Acad Sci U S A* 2004, **101**:5339–46.

103. Seluanov A, Vaidya A, Gorbunova V: **Establishing Primary Adult Fibroblast Cultures From Rodents**. *J Vis Exp* 2010, doi:10.3791/2033.

104. Plubell DL, Wilmarth PA, Zhao Y, Fenton AM, Minnier J, Reddy AP, Klimek J, Yang X, David LL, Pamir N: **Extended Multiplexing of Tandem Mass Tags (TMT) Labeling Reveals Age and High Fat Diet Specific Proteome Changes in Mouse Epididymal Adipose Tissue**. *Mol Cell Proteomics* 2017, **16**:873–890.

105. Thaben PF, Westermark PO: **Detecting rhythms in time series with rain**. *J Biol Rhythms* 2014, **29**:391–400.

106. Plitzko B, Kaweesa EN, Loesgen S: **The natural product mensacarcin induces mitochondrial toxicity and apoptosis in melanoma cells.** *J Biol Chem* 2017, **292**:21102–21116.

107. Plitzko B, Loesgen S: **Measurement of Oxygen Consumption Rate (OCR) and Extracellular Acidification Rate (ECAR) in Culture Cells for Assessment of the Energy Metabolism**. *BIO-PROTOCOL* 2018, **8**.

108. McShane E, Sin C, Zauber H, Wells JN, Donnelly N, Wang X, Hou J, Chen W, Storchova Z, Marsh JA, et al.: **Kinetic Analysis of Protein Stability Reveals Age-Dependent**

Degradation. *Cell* 2016, **167**:803-815.e21.

Supplementary figures

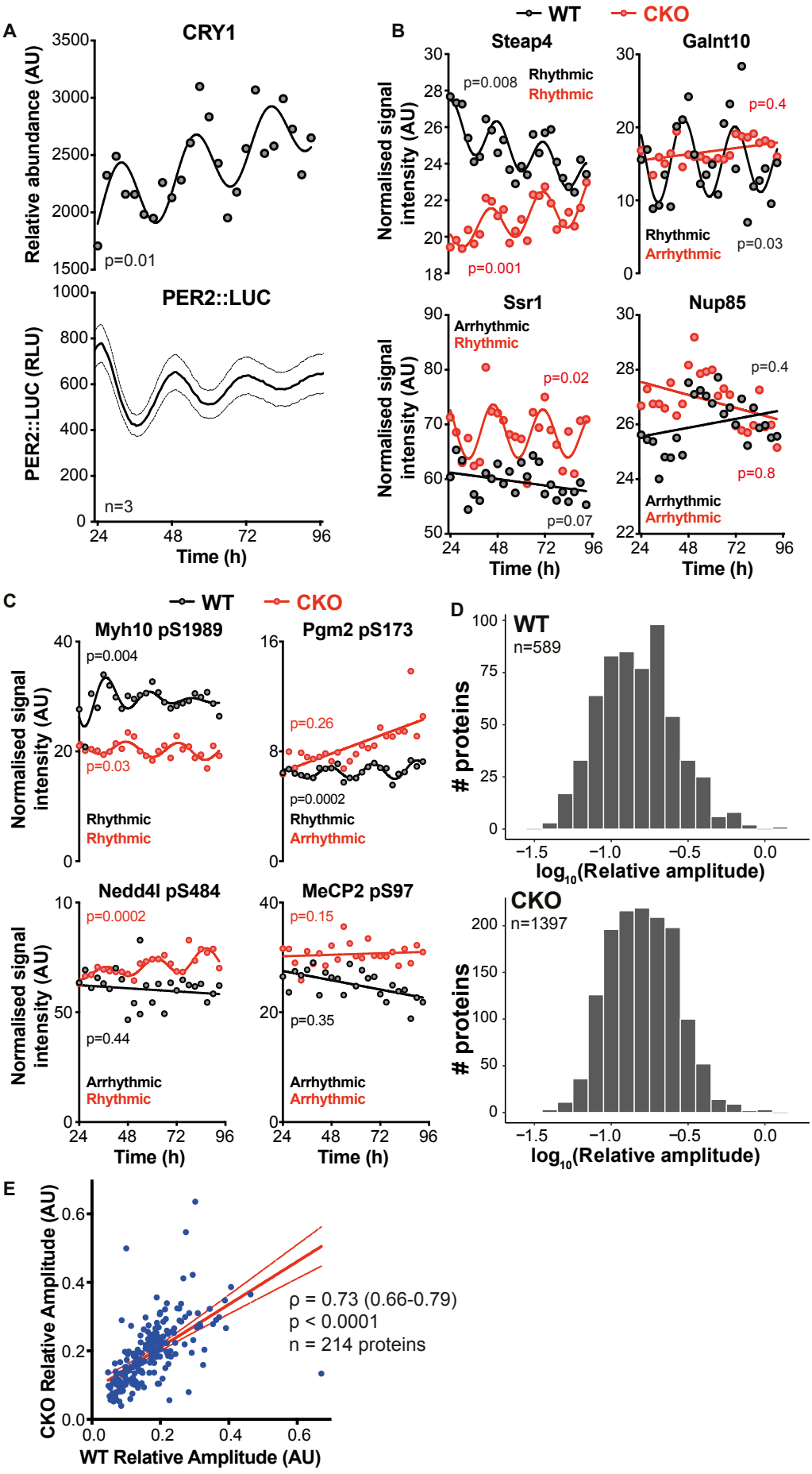

Figure S1. Benchmarking and comparing relative amplitudes of the rhythmic proteome

A) The relative abundance of CRY1 detected in the WT dataset is plotted. It was preferentially fit by a damped cosine wave over a straight line (Extra sum-of-squares F test, p=0.01). Below: Longitudinal bioluminescence recording of WT PER2::LUC fibroblasts, performed simultaneously with the proteomics experiment as a phase marker. Mean±SEM.

B) Examples of proteins detected by mass spectrometry are shown, labelled by gene name. Examples are included of proteins that are rhythmic in both genotypes, rhythmic in only one genotype, or not rhythmic in either. P-values shown are from a comparison of fit (F test, damped cosine against straight line). Annotation as rhythmic/arrhythmic are from the RAIN output.

C) Examples of phosphopeptides detected by mass spectrometry are shown, labelled by gene name and phosphosite. Examples are included of phosphopeptides that are rhythmic in both genotypes, rhythmic in only one genotype, or not rhythmic in either. Annotation as in B).

D) Histograms showing the frequency distributions of relative amplitudes of proteins in WT and CKO cells. The median relative amplitude was significantly higher in CKO cells compared to WT (p=0.008, Kolmogorov-Smirnov test), although the difference was small (WT median = 0.15, CKO median = 0.16).

E) The relative amplitudes of all proteins rhythmic (without the 10% threshold applied) in both WT and CKO cells were plotted, showing a positive correlation between the genotypes. Spearman correlation coefficient (ρ) = 0.73 (95% confidence interval 0.66-0.79), $p < 0.0001$, n = 214 proteins. In red, the linear regression line is plotted with 95% confidence interval.

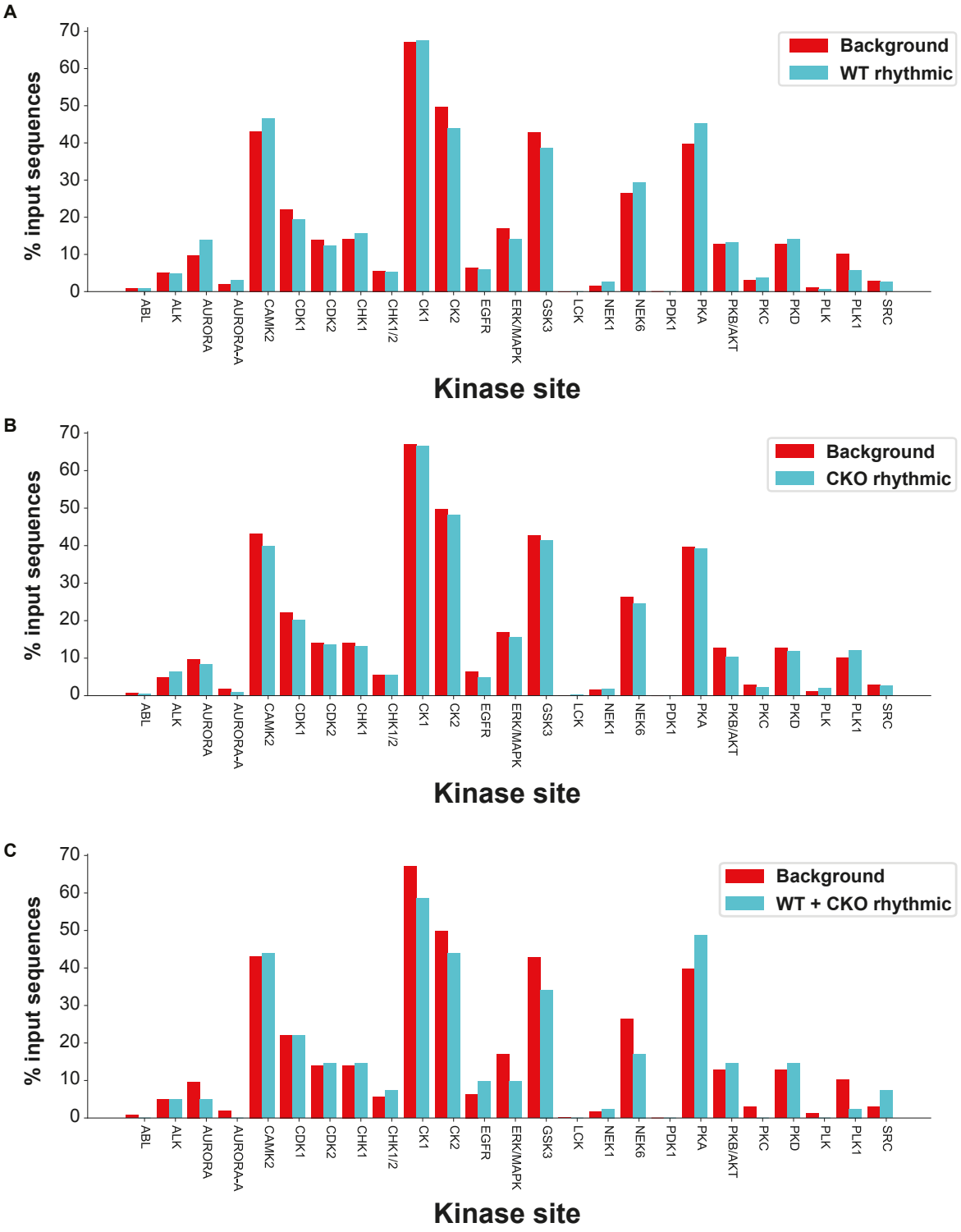

Figure S2. Kinase inference from phosphopeptides in WT and CKO cells

A), B, C) Using the phosphoproteomics dataset, phosphopeptide sequences were analysed, with the number of kinase binding motifs counted for a panel of 25 kinases present in the PHOSIDA database [37,38]. Phosphopeptides that were rhythmic (in WT, in CKO, or in both genotypes respectively) were compared to the background of phosphopeptides present in all samples and pools.

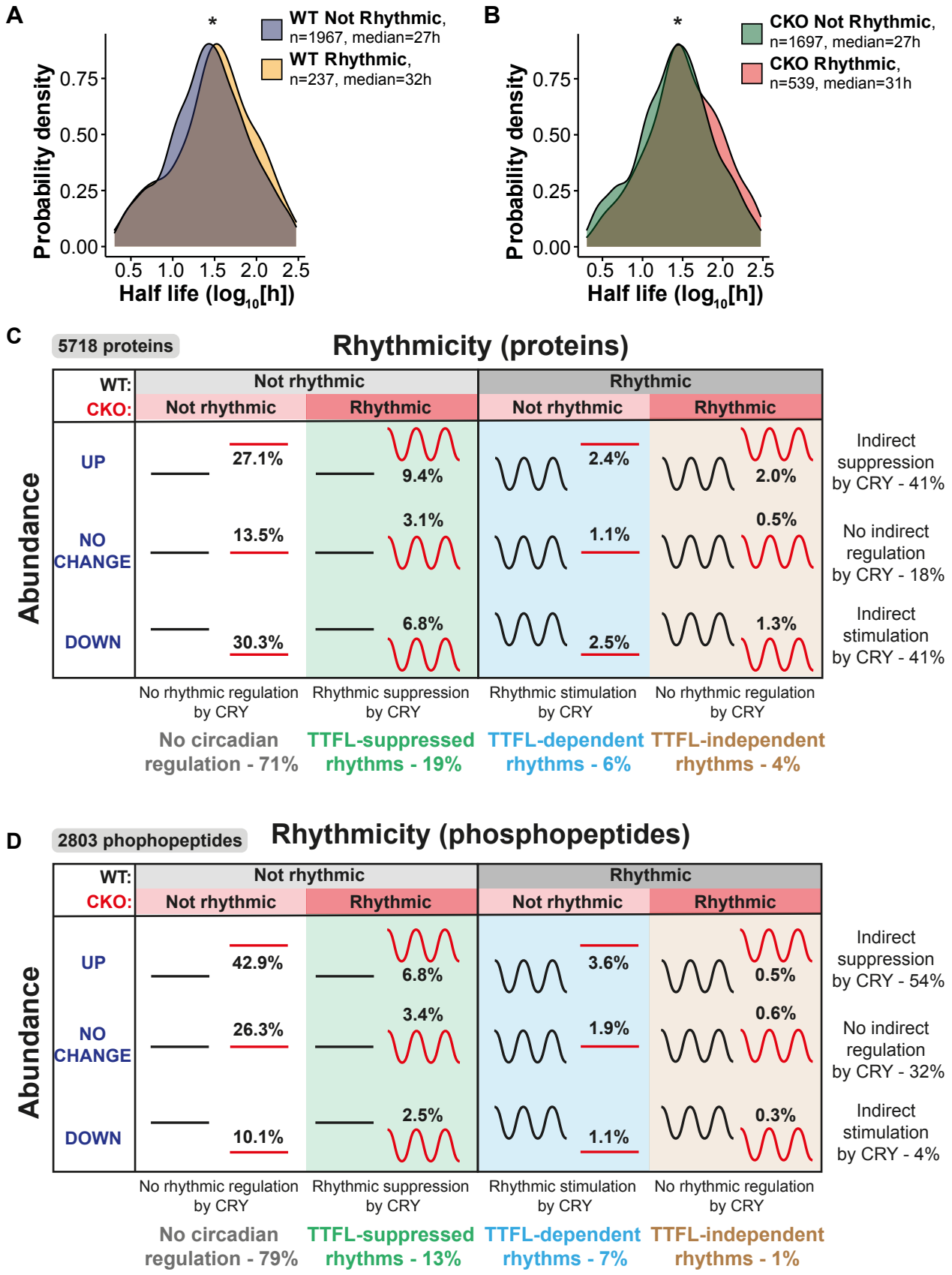

Figure S3. CRY suppresses the proteome and phosphoproteome

A), B) Probability density graphs compare the distribution of protein half-life between rhythmic and non-rhythmic proteins. Half-life was calculated using data from McShane et al. [108]. In both

genotypes, the difference in half-life was statistically significant (WT p=0.04, CKO p=0.01, boot-strapped Kolmogorov-Smirnov test), but many proteins in our dataset were not present in the published dataset. Medians (med): WT rhythmic = 32h, WT non-rhythmic = 27h, CKO rhythmic = 31h, CKO non-rhythmic = 27h.

C) Table summarising the numbers of proteins detected in both genotypes with significantly increased or decreased abundance (corrected $p<0.05$ vs. $p\geq0.05$) and significant change in rhythmicity (RAIN $p<0.05$ vs. $p\geq0.05$) between WT and CKO cells. Rhythms in the abundance of more proteins are suppressed by CRY than are dependent on CRY, and the abundance of most detected proteins changes as a consequence of CRY deletion. There was a significant association between change in abundance and change in rhythmicity (Fisher's exact test, p=0.04).

D) Table summarising the numbers of phosphopeptides detected in both genotypes with significantly increased or decreased abundance (corrected $p<0.05$ vs. $p\geq0.05$) and significant change in rhythmicity (RAIN $p<0.05$ vs. $p\geq0.05$) between WT and CKO cells. More rhythms in protein phosphorylation are suppressed by CRY than are facilitated by CRY, and most detected protein phosphorylation changes as a consequence of CRY deletion. There was a significant association between change in abundance and change in rhythmicity (Fisher's exact test, p=0.009).

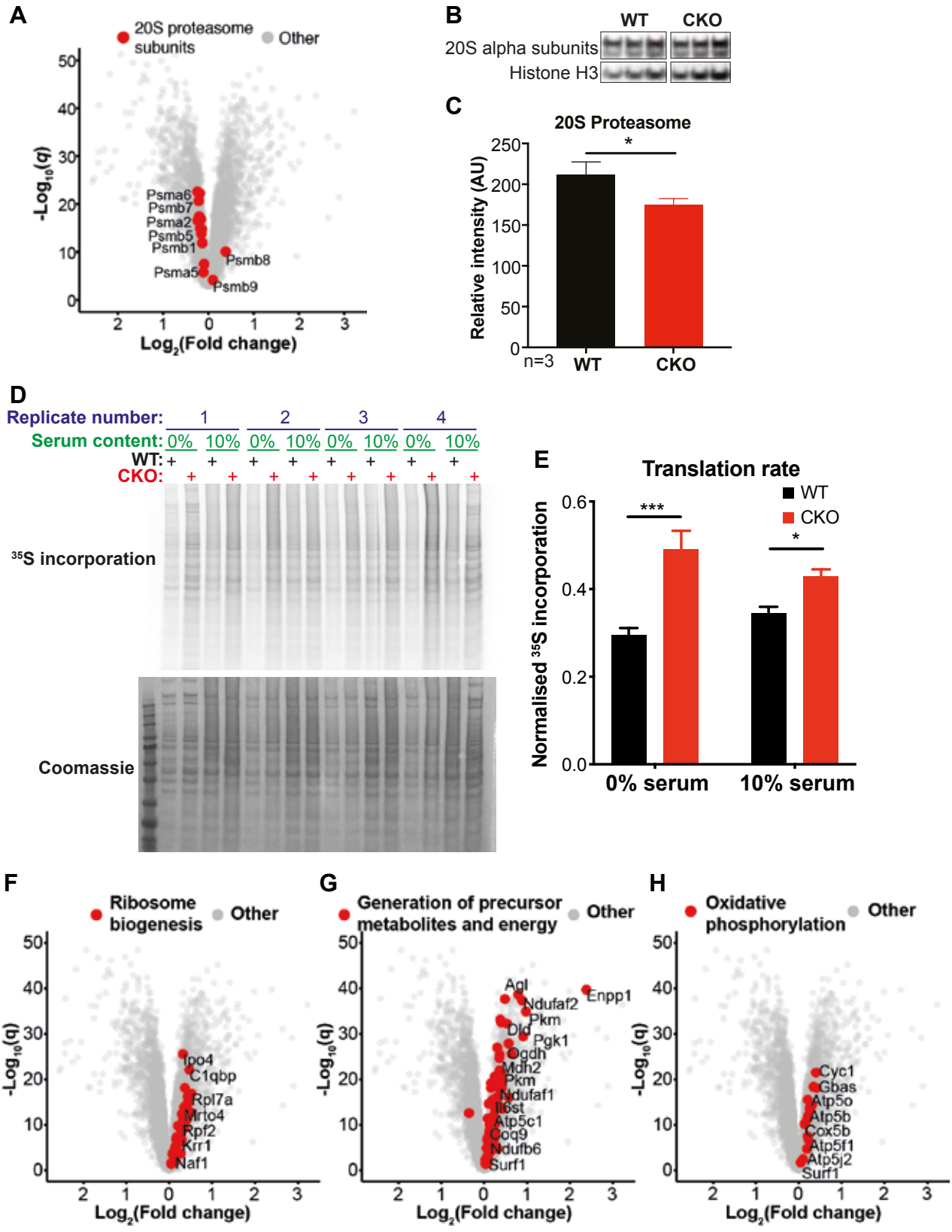

Figure S4. CKO cells have fewer 20S proteasomes, increased translation rate, and upregulated energy generation protein expression

A) Volcano plot showing the fold change in average expression of all proteins in CKO cells compared to WT (*q* = Benjamini-Hochberg corrected p-value). 20S proteasome subunits are highlighted in red, showing that most of these subunits are downregulated in CKO cells.

B) Representative Western blot using an antibody that recognises all 7 α subunits of the 20S proteasome, with anti-histone H3 as loading control.

C) Quantification of the blots in B), using all replicates. Mean±SEM, Student's t test with Welch correction.

D) ^{35}S-methionine incorporation was used to measure translation rate in cultured WT and CKO cells. This was carried out at 0% and 10% serum. 4 replicates are shown, run on the same gel. An image of the phosphor screen is shown above, with the corresponding Coomassie stain below. The condition with 10% serum is shown in Figure 2 as this represents normal culture conditions.

E) Quantification of D). 2-way ANOVA showed interaction between the effects of serum and genotype (p=0.045). Holm-Sidak multiple comparisons results are shown as asterisks. N=3.

F), G), H) Volcano plots illustrate the upregulation of proteins classed in the GO terms: ribosome biogenesis, generation of precursor metabolites and energy, oxidative phosphorylation. Proteins that are classified under each GO term are highlighted in red, whilst all other proteins are shown in grey. Gene names of the proteins are labelled, within the constraints of space.

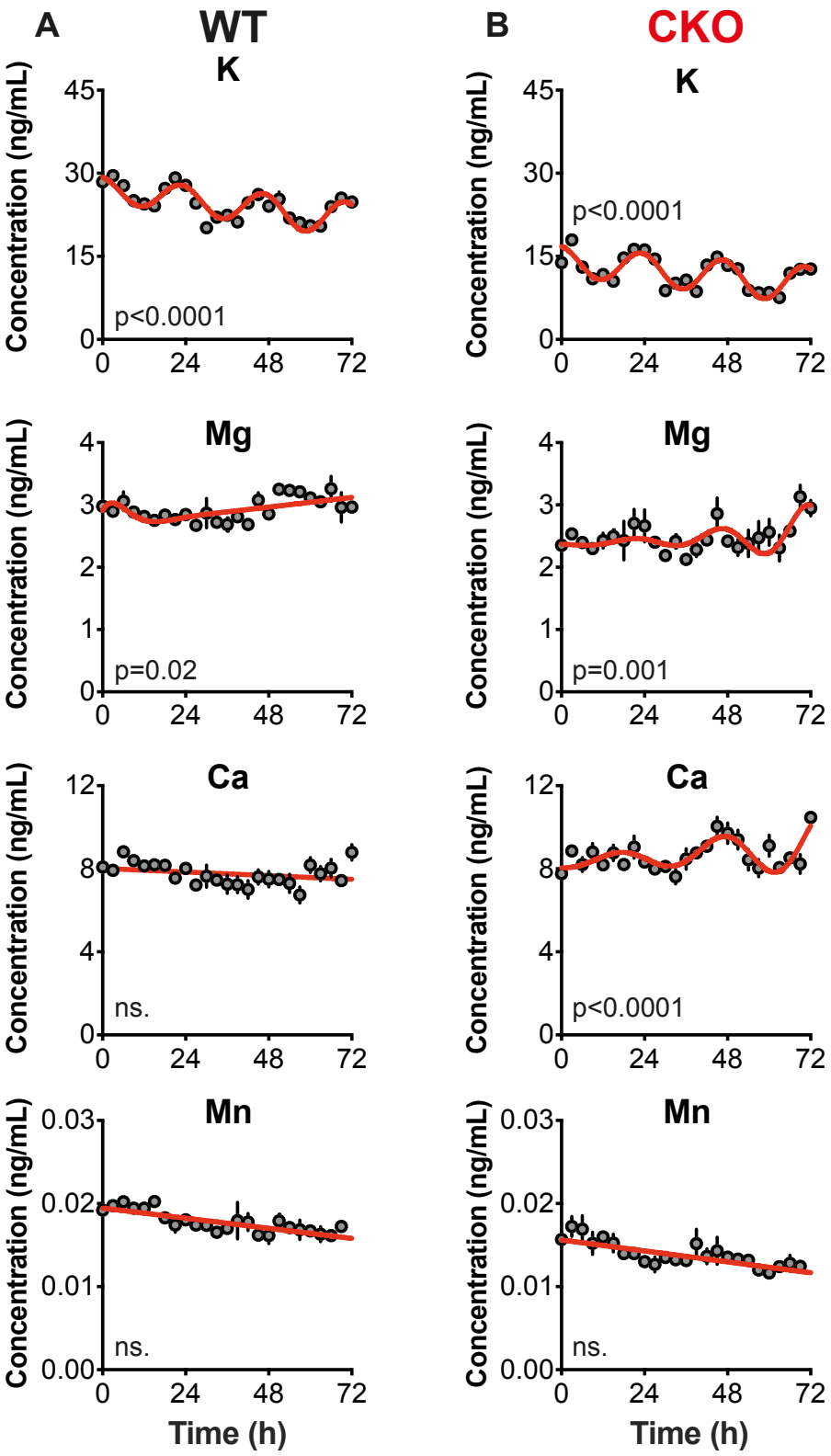

Figure S5. ICP-MS measurement of cellular ion content in CKO and WT cells

A), B) Examples of ions detected from both WT and CKO cells by ICP-MS are shown. Mean±SEM, F test for comparison of fit between damped cosine and straight line, N=3. The preferred fit is shown in red.

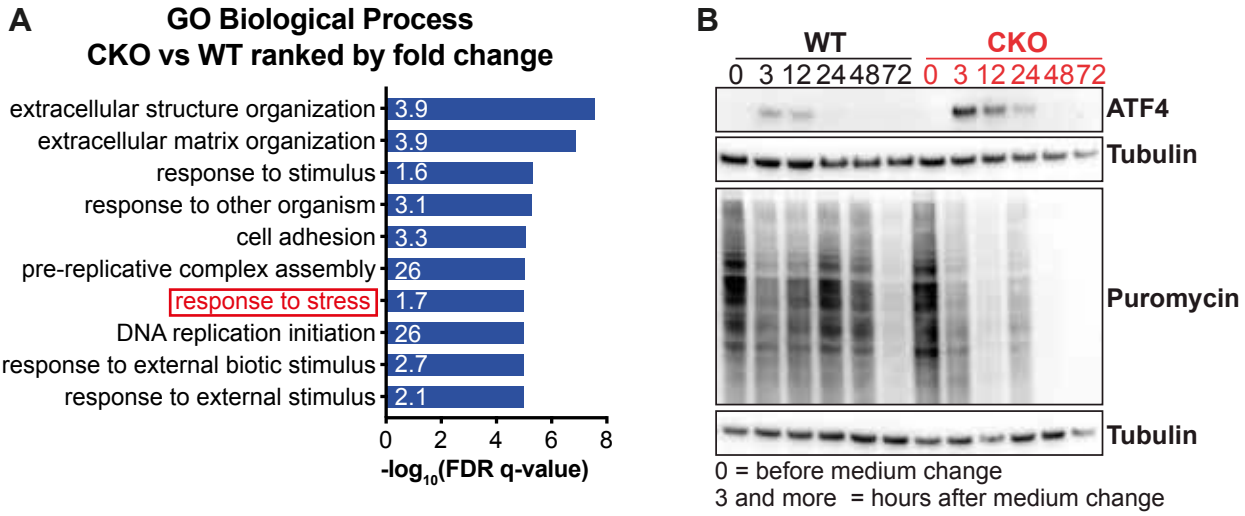

Figure S6. Increased stress response in CKO cells

A) Ranked gene ontology for Biological Process was analysed using a list of all the detected proteins in the proteomics experiment, ranked according to fold change in average expression in CKO cells relative to WT. The top GO terms by FDR q-value are shown, with fold-enrichment annotated.

B) Western blot showing an increased stress response in response to a medium change in CKO cells compared to WT. Cultured cells had the medium changed at time 0 hours into "air medium" (see Methods), and at each time point indicated a puromycin pulse was applied before lysing the cells to measure translation rate. ATF4 is a marker of the integrated stress response, and Tubulin is the loading control.